ASSESSMENT OF AN ITERATIVE APPROACH FOR SOLUTION OF FREQUENCY DOMAIN LINEARIZED EULER EQUATIONS FOR NOISE PROPAGATION THROUGH TURBOFAN JET FLOWS

A THESIS SUBMITTED TO
THE GRADUATE SCHOOL OF NATURAL AND APPLIED SCIENCES
OF
MIDDLE EAST TECHNICAL UNIVERSITY

BY

İLKE EVRİM DİZEMEN

IN PARTIAL FULFILLMENT OF THE REQUIREMENTS

FOR

THE DEGREE OF MASTER OF SCIENCE

IN

AEROSPACE ENGINEERING

DECEMBER 2007

Approval of the thesis:

ASSESSMENT OF AN ITERATIVE APPROACH FOR SOLUTION OF FREQUENCY DOMAIN LINEARIZED EULER EQUATIONS FOR NOISE PROPAGATION THROUGH TURBOFAN JET FLOWS

submitted by **İLKE EVRİM DİZEMEN** in partial fulfillment of the requirements for the degree of **Master of Science in Aerospace Engineering Department,**
Middle East Technical University by,

Prof. Dr. Canan Özgen _____
Dean, Gradute School of **Natural and Applied Sciences**

Prof. Dr. İsmail Hakkı Tuncer _____
Head of Department, **Aerospace Engineering**

Prof. Dr. Yusuf Özyörük _____
Supervisor, **Aerospace Engineering Dept., METU**

Examining Committee Members:

Prof. Dr. İsmail Hakkı Tuncer
Aerospace Engineering Dept., METU _____

Prof. Dr. Yusuf Özyörük
Aerospace Engineering Dept., METU _____

Asst. Prof. Dr. Oğuz Uzol
Aerospace Engineering Dept., METU _____

Prof. Dr. Zülfü Aşık
Engineering Sciences Dept., METU _____

Dr. Nilay Sezer Uzol
Mechanical Engineering Dept., TOBB ETU _____

Date: _____

I hereby declare that all information in this document has been obtained and presented in accordance with academic rules and ethical conduct. I also declare that, as required by these rules and conduct, I have fully cited and referenced all material and results that are not original to this work.

Name, Last Name: İlke Evrim Dizemen

Signature :

ABSTRACT

ASSESSMENT OF AN ITERATIVE APPROACH FOR SOLUTION OF FREQUENCY DOMAIN LINEARIZED EULER EQUATIONS FOR NOISE PROPAGATION THROUGH TURBOFAN JET FLOWS

Dizemen, İlke Evrim

M.S., Department of Aerospace Engineering

Supervisor: Prof. Dr. Yusuf Özyörük

December 2007, 45 pages

This study, explores the use of an iterative solution approach for the linearized Euler equations formulated in the frequency domain for fan tone noise propagation and radiation through bypass jets. The aim is to be able to simulate high frequency propagation and radiation phenomena with this code, without excessive computational resources. All computations are performed in parallel using MPI library routines on a computer cluster. The linearized Euler equations support the Kelvin-Helmholtz type convective physical instabilities in jet shear flows. If these equations are solved directly in frequency domain, the unstable modes may be filtered out for the frequencies of interest. However, direct solutions are memory intensive and the reachable frequency is limited. Results provided shown that iterative solution of LEE is more efficient when considered memory requirement and might solve a wider scope of frequencies, if the instabilities are controlled.

Keywords: Aeroacoustic, Propagation, Iterative Methods, Frequency Domain, Kelvin-Helmholtz Instability.

ÖZ

TURBOFAN JET AKIŞLARI BOYUNCA YAYILAN GÜRÜLTÜNÜN FREKANS ALANINDA DOĞRUSALLAŞTIRILMIŞ EULER DENKLEMLERİ İLE ÇÖZÜMÜNDE YENİLEMELİ YÖNTEMİN DEĞERLENDİRİLMESİ

Dizemen, İlke Evrim

Yüksek Lisans, Havacılık ve Uzay Mühendisliği Bölümü

Tez Yöneticisi: Prof. Dr. Yusuf Özyörük

Aralık 2007, 45 sayfa

Bu çalışmada, paralel jet akışları boyunca yayılan gürültünün frekans alanında doğrusallaştırılmış Euler denklemleri (DED) ile çözümünde yenilemeli yöntemin kullanımı incelenmiştir. Geliştirilen kod ile yüksek frekanslarda sesin yayılımını aşırı bilgisayar gücü gerektirmeden modellemek amaçlandı. Bütün hesaplamalar MPI kütüphanesı kullanılarak gerçekleştirildi. Doğrusallaştırılmış Euler denklemleri jet akışı karışım bölgesinde Kelvin-Helmholtz tipi yayılan fiziksel düzensizlikleri desteklemektedir. Bu denklemler frekans alanında doğrudan çözüldüğü taktirde incelenen frekanslar için bu düzensizlikler elenebilir. Ancak doğrudan çözümler bilgisayar hafızası ihtiyacı açsından hasastır ve çözülebilen frekans aralığı limitlidir. Sunulan sonuçlar DED'nin yenilemeli yöntem ile çözümünün bilgisayar hafızası ihtiyacı ve daha geniş bir frekans aralığında çözüm elde edilebilmesi göz önüne alındığında düzensizliklerin daha verimli kontrol edildiğini göstermektedir.

Anahtar Kelimeler: Aeroakustik, Yayılma, Yenilemeli Metod; Frekans Alanı, Kelvin-Helmhotz Düzensizliği.

to my family...

ACKNOWLEDGMENTS

I want to state my thanks to

My thesis supervisor *Prof. Dr. Yusuf Özyörük* for his guidance and valuable sharing through out this study with patience.

My parents for their advice and supports in my life, being with me anytime and anywhere that I need help and courage. **My father** for being the only reason to finish that study. **My mother** for her prays and trust. **My sister** for always believing in me more then myself.

My assistant friends Mustafa Kaya, for his helps and guidance in code programming, Tahir Turgut for his great LaTeX assistance and Barbaros Ulusoy for his useful discussions.

My all friends for their incredible support and gaz.

PREFACE

The sound radiation became a critical issue with increasing air traffic. Researchers in this area cleared some aspects of noise radiation from aircraft problem. Today, although the developed methods are qualified the noise restrictions around some airports force researches to make quieter models. Frequency domain proved its ability on impedance boundaries. The iterative method applied in this study also help the method to make simulate noise radiation with less computational memory requirements.

You can report all comments to the following e-mail address:

İlke Evrim Dizemen

gudik@ae.metu.edu.tr

All comments are welcome.

METU, Ankara

January 2008

TABLE OF CONTENTS

LIST OF TABLES

TABLES

LIST OF FIGURES

FIGURES

LIST OF SYMBOLS

ROMAN SYMBOLS

B	Number of rotor blades
c	Speed of sound
D	Artificial dissipation
f	Frequency in Hertz
i	Complex number,$\sqrt{-1}$
J_m	m^{th} order Bessel Function of first kind
J'_m, Y'_m	derivatives of Bessel Functions with respect to r
k	Wave number
$k_{m,\mu}$	Eigenvalues of transcendental equation
L_{ref}	Length of Buffer zone
L_x	Length of Buffer zone in axial direction
L_r	Length of Buffer zone in radial direction
m	Azimuthal mode
M	Mach Number
n	Time harmonic index
r	Radial distance in Cylindrical system
R	Radius of wall curvature
Rhs	Residual matrix
S	Kirchhoff surface
q	Solution vector
t	Time
u	Velocity component in x-direction
U	Jet flow velocity
Y_m	m^{th} order Bessel Function of second kind
v	Velocity component in y-direction
V	Number of stator vanes
V	Uniform mean flow velocity
w	Velocity component in z-direction
x, y, z	Spatial coordinates in Cartesian system
x_i, r_i	Location of PML/EULER interface in axial and radial directions

GREEK SYMBOLS

$\Re$	Real part of the variable
γ	Specific heat ratio
θ	Angular coordinate in Cylindrical system
θ_m	Momentum thickness of shear layer
ω	Circular frequency
ρ	Density
μ	Radial mode
σ	Hub to tip ratio
$\sigma(x)$	Transition coefficient
ξ_{mn}	Cut-off ratio
τ	Pseudo term; source emission time
$\delta\tau$	Pseudo time step size
ξ, η	Spatial coordinates in computational domain
$\xi_x, \xi_z,$ η_x, η_z	Metrics of transformation

SUBSCRIPTS

∞	Freestream value
0	Mean flow quantitiy
b	By-pass stream value
c	Core stream value

f	Freestream value
inc, in	Incident field
n	Normal component of velocity
re	Reflected field
t	Tangential component of velocity

SUPERSCRIPTS

$'$	Perturbation
$\widehat{\ }$	Complex quantity, Incident field variables
$+$	Acoustic Wave going in downstream direction
n	Time integral step

CHAPTER 1

INTRODUCTION

1.1 Introduction

Modern airliners of today are commonly using turbofan engines. Due to the increasing by-pass ratio, fan diameter and fan loads the sound generated by and propagated from the turbofan engines increased significantly. This high noise level of turbofan engines is an important problem for the passengers onboard and the people living around airports. Especially for the people living under the the takeoff/landing pattern of airports (as shown in fig. 1.1) the noise levels of turbofan engines may be unacceptable during intense air traffic hours. Hence, noise emission from turbofan engines is an up-to-date topic of research. But there is still a need for significant effort to reduce the sound emitted from the exhaust section of turbofan engines. There are various challenges in predicting noise propagation and radiation through highly nonuniform exhaust flows of such engines. The prediction of sound from such flows has two stages. One is the characterization of the source which is in the scope of generation studies and the other is the propagation through the sheared layer. The real challenge of the noise emitted by exhaust section of turbofan engines is there occurs in a jet mixing layer. Noise issuing from an exhaust duct must propagate through jet shear layers before it radiates to far-field as shown in fig. 1.2 from [2]. Prediction of noise propagation through jets is not straightforward, as shear related physical instabilities may be captured and alias propagated fan tones.

Figure 1.1: ICAO Annex 16 Certification, take-off and landing profile [1].

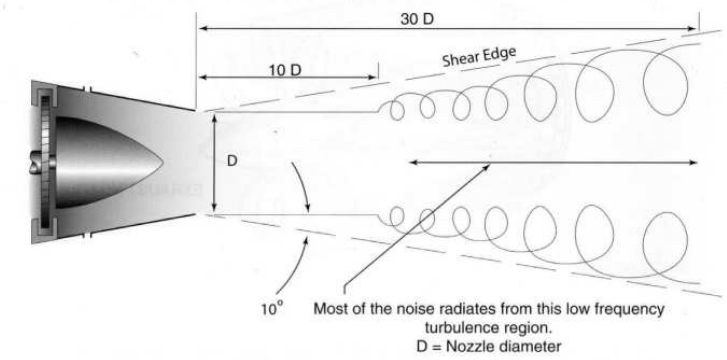

Figure 1.2: Jet Noise Schematic [2].

Acoustic perturbations are so small compared to the background (mean) flow that their contribution to the unsteady jet flow itself is negligible as stated by P.J. Morris *et al.* [3]. Therefore acoustic waves can be described by using linearized flow equations. Additionally, since the viscosity has a negligible effect on sound propagation, the viscous terms can also be neglected. Neglecting the viscous terms from flow equations results in the Euler equations. By linearizing the Euler equations about a time averaged flow (namely background or mean flow) one can realistically describe the sound propagation in a moving medium.

However, in addition to sound waves, the linearized Euler equations also support convective instabilities that, for a jet, are known as Kelvin-Helmholtz instabilities [3]. In a temporal calculation these convective instabilities can completely ruin the acoustic wave solution as they propagate downstream. On the contrary, direct solution of LEE in frequency domain does not

support the Kelvin-Helmholtz instability waves as shown by P.J. Morris *et al.* [3]. However, the direct solution of LEE equations require excessive computational resources, in particular memory. Memory need for an example calculation with a direct method in frequency domain using SuperLU and MUMPS are shown by Özyörük and Dizemen [4] as in Table 1.1.

Table 1.1: Direct Solution Results

CASE	SuperLU		MUMPS	
	Peak memory per process (Mb.)	Wall clock time (seconds)	Peak memory per process (Mb.)	Wall clock time (seconds)
1	85	152	126	25
2	442	466	459	76
3	3994	6371	2533	451

Iterative solution of LEE in frequency domain can be considered when the computational power is the matter of concern. With decreased memory requirement larger solution domains or higher frequencies can be investigated. However, iterative solution might support instability waves and can ruin the solution at some frequencies. As shown by Michalke [5] radiation throughout an inviscid shear layer will be stable if the frequency of the acoustic wave is large enough. Assuming an incompressible, isothermal, parallel shear layer between a jet and a fluid at rest for stable solution the frequency of the acoustic wave should satisfy

$$\frac{\omega\theta_m}{U_0} > 0.25 \tag{1.1}$$

where θ_m is the momentum thickness of the shear layer, U_0 is the jet velocity and ω is the circular frequency. Using the formula of Michalke one can predict the minimum frequency of the acoustic wave that might be solved using LEE without running into Kelvin-Helmholtz instabilities. It should be noted that the formula of Michalke is valid if the shear layer is thin enough, namely $\theta_m < 0.08R$ where R is the jet radius.

1.2 Thesis Scope and Outline

The scope of this study is to develop an iterative solution approach for the linearized Euler equations formulated in the frequency domain for fan tone noise propagation and radiation through bypass jets. The aim is to be able to see the frequency capabilities of an iterative

method in solution of propagation and radiation through high speed jets mixing layer, without excessive computational resources and filtering the instability waves. There are several possibilities for iterative approaches in the literature. Linearization of the Euler equations is made about a mean flow that comes from CFD solutions, so that its effects on sound propagation are included in computations more realistically. In the present study the iterative approach described by Y.B. Ulusoy [6] is extended to realistic engine geometries. Parallelization methodology of distributed memory architectures with domain decomposition and the Message Passing Interface (MPI) for inter-processor communications appliedin this code. Solution domain is divided into subdomains of nearly equal grid point loads for equal solution times among the subdomains. The equality of the solution time is important since the lag between the communication of each subdomain might significantly increase the overall solution time. It would be particularly important for exhaust radiation from turbofans that the shear layer emanating from the shroud of the engine may cause significant diffraction and refraction of the emitted sound waves. Hence, mathematical modelling of the shear layer growing throughout the trailing edge of exhaust nacelles has great importance.

Today, either experimental or 3-D numerical direct methods are so difficult to handle. Frequency domain approach may be applied with an iterative method for the solution of system of equations. Direct solution of discretized equations also requires large amount of memory which limits the reachable size of the solution domain.

Chapter 2 is about Mathematical Model applied throughout this study. In the chapter, frequency domain equations are given. Applied Kirchhoff technique and boundary conditions are also described in the chapter.

Chapter 3 describes the Numerical Method for solutions. This chapter also contains description of the parallel processing strategy applied.

Chapter 4 presents the results of and discussion on the test cases. This chapter also contains the comparison of test cases with the results of the direct frequency domain LEE solver FLESTURN developed by Özyörük *et al.* [7].

Chapter 5 will include conclusions from the study from a physical and numerical aspect.

CHAPTER 2

MATHEMATICAL MODEL

2.1 Introduction

In this chapter, the mathematical model employed to compute the frequency domain solution of turbofan noise is summarized. In general, a mean flow is computed for steady state conditions. Then, the obtained background flow is used for frequency domain solution. The full solution domain is divided into sub-zones. The computations for each sub-zone are performed in parallel. MPI message passing library routines are used in the parallel solution algorithm. For far-field prediction Kirchhoff method is used. Additionally, non-reflecting boundary conditions , namely Perfectly Matching Layer (PML) and Asymptotic Characteristic Based conditions are applied to the far-field and duct inlet boundaries to defeat the wave reflections from these boundaries. A generic overview of the solution domain is shown in figure 2.1.

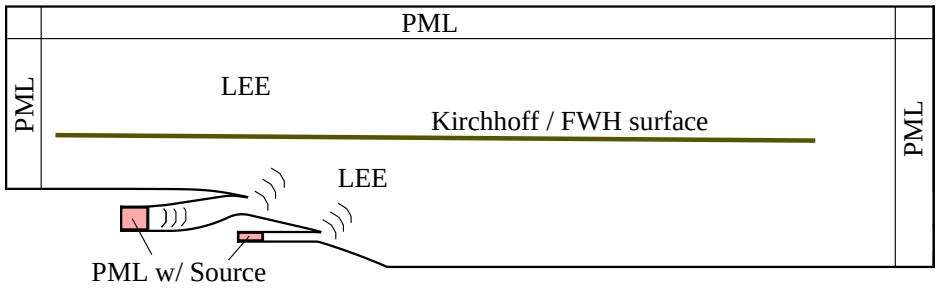

Figure 2.1: General configuration.

2.2 Governing Equations

2.2.1 Linearized Euler Equation

The linearized equations are given in cylindrical co-ordinates by,

$$\begin{aligned}
&\frac{\partial \rho'}{\partial t} + \rho_0\left(\frac{\partial u'}{\partial x} + \frac{\partial v'}{\partial r} + \frac{v'}{r} + \frac{1}{r}\frac{\partial w'}{\partial \theta}\right) + u_0\frac{\partial \rho'}{\partial x} + v_0\left(\frac{\partial \rho'}{\partial r} + \frac{\rho'}{r}\right) + \rho'\left(\frac{\partial u_0}{\partial x} + \frac{\partial v_0}{\partial r}\right) + u'\frac{\partial \rho_0}{\partial x} + v'\frac{\partial \rho_0}{\partial r} = 0 \\
&\frac{\partial u'}{\partial t} + u_0\frac{\partial u'}{\partial x} + v_0\frac{\partial u'}{\partial r} + u'\frac{\partial u_0}{\partial x} + v'\frac{\partial u_0}{\partial r} + \frac{1}{\rho_0}\frac{\partial p'}{\partial x} = 0 \\
&\frac{\partial v'}{\partial t} + u_0\frac{\partial v'}{\partial x} + v_0\frac{\partial v'}{\partial r} + u'\frac{\partial v_0}{\partial x} + v'\frac{\partial v_0}{\partial r} + \frac{1}{\rho_0}\frac{\partial p'}{\partial x} = 0 \\
&\frac{\partial w'}{\partial t} + u_0\frac{\partial w'}{\partial x} + v_0\frac{\partial w'}{\partial r} + \frac{1}{\rho_0 r}\frac{\partial p'}{\partial \theta} + \frac{v_0 w'}{r} = 0 \\
&\frac{\partial p'}{\partial t} + u_0\frac{\partial p'}{\partial x} + v_0\frac{\partial w'}{\partial r} + u'\frac{\partial p_0}{\partial x} + v'\frac{\partial p_0}{\partial r} + \gamma p_0\left(\frac{\partial u'}{\partial x} + \frac{\partial v'}{\partial r} + \frac{v'}{r} + \frac{1}{r}\frac{\partial u'}{\partial \theta}\right) + \gamma p'\left(\frac{\partial u_0}{\partial r} + \frac{\partial v_0}{\partial r} + \frac{v_0}{r}\right) = 0
\end{aligned} \tag{2.1}$$

The 3-D, time domain, LEE equations are transformed into the frequency domain assuming that perturbations of the primitive-dependent variables of the form;

$$q'(x,t) = \Re\left[\widehat{q}\,(x,r,\omega)e^{i\omega t + im\theta}\right] \tag{2.2}$$

where,

$$q' = [\rho', u', v', w', p']^T,\ \widehat{q} = [\widehat{\rho}, \widehat{u}, \widehat{v}, \widehat{w}, \widehat{p}]^T \tag{2.3}$$

and $i = \sqrt{-1}$, ρ', u', v', w', p' are density, velocity and pressure perturbations, respectively, in the cylindrical (x,r,θ) coordinates. A hat on the variable indicates a complex quantity. In Equation 2.2, ω is the circular frequency and integer m represents the azimuthal mode number.

Substitution of equation 2.2 into the linearized Euler equations 2.1, in cylindrical co-ordinates the equations governing the complex amplitudes of the flow perturbations become,

$$
\begin{aligned}
&i\omega\widehat{\rho} + \rho_0\frac{\partial\widehat{v}}{\partial r} + \widehat{v}\frac{\partial\rho_0}{\partial r} + v_0\frac{\partial\widehat{v}}{\partial r} + \widehat{\rho}\frac{\partial v_0}{\partial r} + \tfrac{1}{r}(\rho_0\widehat{v} + v_0\widehat{\rho}) + \rho_0\frac{\partial\widehat{u}}{\partial x} + \widehat{u}\frac{\partial\rho_0}{\partial x} + u_0\frac{\partial\widehat{\rho}}{\partial x} + \widehat{\rho}\frac{\partial u_0}{\partial x} + \rho_0\frac{im}{r}\widehat{w} = 0\\
&i\omega\widehat{u} + u_0\frac{\partial\widehat{u}}{\partial x} + v_0\frac{\partial\widehat{u}}{\partial r} + \widehat{u}\frac{\partial u_0}{\partial x} + \widehat{v}\frac{\partial u_0}{\partial r} + \frac{1}{\rho_0}\frac{\partial\widehat{p}}{\partial x} = 0\\
&i\omega\widehat{v} + u_0\frac{\partial\widehat{v}}{\partial x} + v_0\frac{\partial\widehat{v}}{\partial r} + \widehat{u}\frac{\partial v_0}{\partial x} + \widehat{v}\frac{\partial v_0}{\partial r} + \frac{1}{\rho_0}\frac{\partial\widehat{p}}{\partial r} = 0\\
&i\omega\widehat{w} + u_0\frac{\partial\widehat{w}}{\partial x} + v_0\frac{\partial\widehat{w}}{\partial r} + \frac{im}{\rho_0 r}\widehat{p} + \frac{v_0\widehat{w}}{r} = 0\\
&i\omega\widehat{p} + u_0\frac{\partial\widehat{p}}{\partial x} + v_0\frac{\partial\widehat{p}}{\partial r} + \widehat{u}\frac{\partial p_0}{\partial x} + \widehat{v}\frac{\partial p_0}{\partial r} + \gamma p_0(\frac{\partial\widehat{u}}{\partial x} + \frac{\partial\widehat{v}}{\partial r} + \frac{\widehat{v}}{r} + \frac{im}{r}\widehat{w}) + \gamma\widehat{p}(\frac{\partial u_0}{\partial x} + \frac{\partial v_0}{\partial r} + \frac{v_0}{r}) = 0
\end{aligned}
\tag{2.4}
$$

where $[\rho_0, u_0, v_0, w_0, p_0]^T$ represent the non-uniform, axisymmetric, mean flow variables. Looking at equation 2.1 and equation 2.4, it can be seen that the latter one contains derivatives only in (x,r). This difference results from azimuthal variations transformed to the terms multiplied by *im*. So frequency domain LEE has less gradient variables to compute, this reduces the computational expense of full 3-D domain.

2.3 Boundary Conditions

In numerical simulations of problems, a set of equations is required to model boundary conditions. These boundary conditions are applied all around the interior computational domain where the flow equations are solved. While applying boundary conditions, the physics of a particular problem must be modelled correctly by required mathematical expressions. For some particular problems, additional numerical boundary conditions may be required. The manner in which boundary conditions are specified must be considered in the overall stability and accuracy of numerical scheme used to solve the system. The boundary conditions can be applied explicitly or implicitly. They must allow the flow disturbances to leave the computational domain without significant reflections. This is crucial in computational aeroacoustic (CAA), since spurious acoustic waves generated by poor boundary condition application may mask the physical sound field radiated. The applied boundary conditions are summarized below.

2.3.1 Acoustic source conditions

In order to excite the acoustic field, exact cylindrical duct eigensolutions are used at the fan face which is assumed to be a deviation from the mean field. To obtain the following equation, wave

equation is written in cylindrical coordinates and with help separation of variables technique general solution in terms of Bessel equations is obtained. Acoustic pressure in hard-walled duct at a constant x plane for a circular annular duct is given by,

$$\widehat{p}(r,\theta) = \sum_{m,\mu} A_{m,\mu}[J_m(k_{m,\mu}r) + Q_{m,\mu}Y_m(k_{m,\mu}r)]e^{i(m\theta)} \tag{2.5}$$

where m and μ are the azimuthal and radial mode orders, respectively; $A_{m,\mu}$ is the amplitude of (m,μ) mode; J_m and Y_m are the m^{th} order Bessel functions of the first and second kinds, respectively; $k_{m,\mu}$ are the eigenvalues that make the transcendental equation zero resulting from the wall condition, $\frac{\partial p}{\partial r}\,|_{wall} = 0$; $A_{m,\mu} = -J'_{m,\mu}(\sigma k_{m,\mu})/Y'_{m,\mu}(\sigma k_{m,\mu})$ in which a prime indicates a derivative with respect to r, and σ is the hub to tip ratio. When there is no center body $Q_{m,\mu}$ is zero. The azimuthal mode order m is found using the rotor stator interaction theory of Taylor and Sofrin [8]. In this theory, the circumferential mode order m is obtained by,

$$m = nB + sV \tag{2.6}$$

where B and V are the number of rotor blades and stator vanes, respectively, n is the time harmonic index and s is any integer number. Once the number of rotor blades, the number of exit guide vanes and the rotor speed are known, the modes that are cut on are determined based on the local mean flow conditions at the source plane.

2.3.1.1 Characteristic-based inlet conditions

The non-reflecting boundary conditions of Giles [9] are adapted to the present work to introduce the incident acoustic waves into the domain while letting outgoing ones leave it with minimal reflection. The adopted conditions are given in the frequency domain by,

$$\begin{aligned}
&i\omega\widehat{u} + \tfrac{u_0+c_0}{2\rho_0 c_0}(\tfrac{\partial\widehat{p}}{\partial x} + \rho_0 c_0 \tfrac{\partial\widehat{u}}{\partial x}) + \tfrac{(c_0-u_0)}{4}(\tfrac{\partial\widehat{v}}{\partial r} + \tfrac{\widehat{v}}{r} + \tfrac{im}{r}\widehat{w}) = i\omega\tfrac{L_1}{\rho_0 c_0}\\
&i\omega\widehat{v} + u_0\tfrac{\partial\widehat{v}}{\partial x} + \tfrac{1}{\rho_0}\tfrac{\partial\widehat{p}}{\partial r} = 0\\
&i\omega\widehat{w} + u_0\tfrac{\partial\widehat{w}}{\partial x} + \tfrac{im}{\rho_0 r}\widehat{p} = 0\\
&i\omega\widehat{p} + \tfrac{u_0+c_0}{2}(\tfrac{\partial\widehat{p}}{\partial x} + \rho_0 c_0 \tfrac{\partial\widehat{u}}{\partial x}) + \tfrac{3c_0+u_0}{4}(\tfrac{\partial\widehat{v}}{\partial r} + \tfrac{\widehat{v}}{r} + \tfrac{im}{r}\widehat{w}) = -i\omega L_1
\end{aligned} \tag{2.7}$$

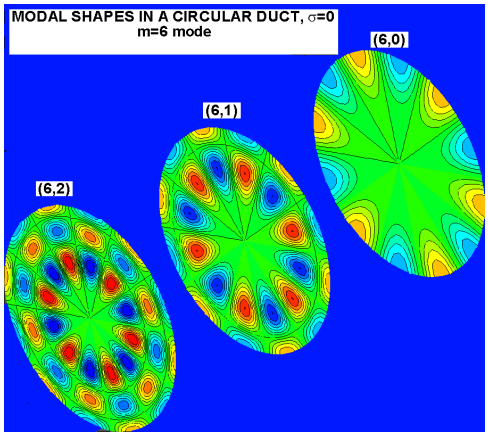

(a) Circular Duct Mode pattern.

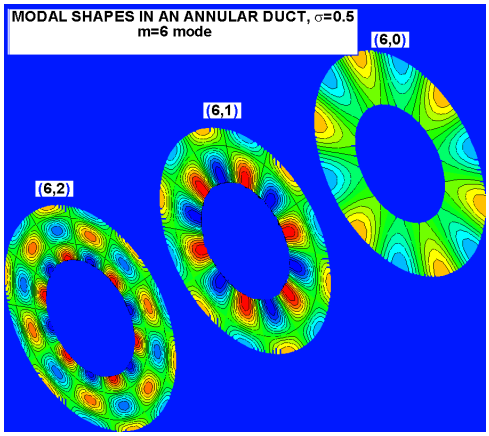

(b) Annular Duct Mode pattern.

Figure 2.2: Circular and Annular Duct Mode pattern for $m = 6$.

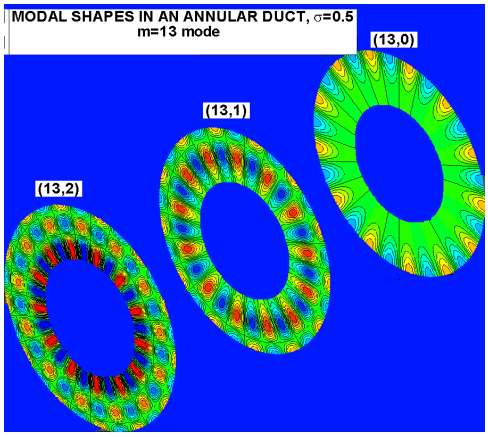

Figure 2.3: Annular Duct Mode pattern for $m = 13$.

where L_1 is set to the incident part of the acoustic pressure that is given by equation 2.5. Numerical experimentation has shown that these conditions do not completely eliminate the outgoing waves [10]. The radial wave number is determined from turning points of the Bessel function, and axial wave number and cut-off ratio are calculated from Equation 2.8 and Equation 2.9 respectively.

$$k_a = (k/\beta^2)(-M_\infty^2 \pm \sqrt{1-\xi^2}) \tag{2.8}$$

$$\xi_{mn} = \frac{k}{\beta k_a},\ \beta = \sqrt{1-M^2} \tag{2.9}$$

As the cutoff ratio approaches 1 for the propagating mode, the propagation angle approaches 90^o, and the mode decays. To propagate, a mode cutoff ratio must be greater than 1. Some

modal shapes are illustrated for annular and circular ducts, Figure 2.2 and Figure 2.3. The mode characterize the pressure pattern propagating in the duct.

2.3.1.2 Perfectly Matching Layer Approach

Perfectly Matching Layer (PML) approach of Hu [11] is applied to the current problem as described in [7], which requires an additional zone of mesh as in buffer zone approach shown in fig. 2.4.

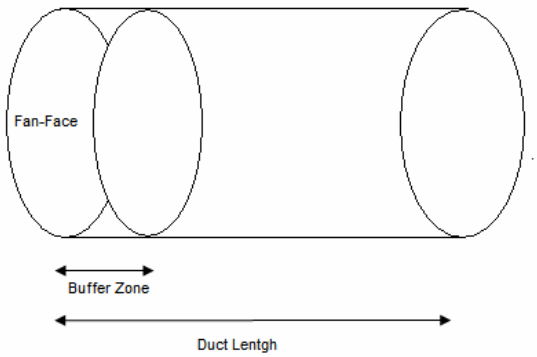

Figure 2.4: Buffer zone in circular duct.

Background flow is assumed uniform at the inlets of the ducts, as well as the far-field boundaries, with a velocity of $\mathbf{V} = u_0\hat{\mathbf{e}}_x$. The PML equations are written in a similar form to the interior LEE if the equations are written in the form

$$[A]\frac{\partial \mathbf{q}}{\partial x} + [B]\frac{\partial \mathbf{q}}{\partial r} + [C]\mathbf{q} = \mathbf{Rhs} \tag{2.10}$$

then the Jacobian matrices are given by

$$[A]_{\text{pml}} = \begin{bmatrix} u_0(1+\frac{\sigma_r}{i\omega}) & \rho_0(1+\frac{\sigma_r}{i\omega}) & 0 & 0 & 0 \\ 0 & u_0(1+\frac{\sigma_r}{i\omega}) & 0 & 0 & \frac{(1+\frac{\sigma_r}{i\omega}}{\rho_0} \\ 0 & 0 & u_0(1+\frac{\sigma_r}{i\omega}) & 0 & \frac{(1+\frac{\sigma_x}{i\omega}}{\rho_0} \\ 0 & 0 & 0 & u_0(1+\frac{\sigma_r}{i\omega}) & 0 \\ 0 & \gamma p_0(1+\frac{\sigma_r}{i\omega}) & 0 & 0 & u_0(1+\frac{\sigma_r}{i\omega}) \end{bmatrix},$$

$$[B]_{\text{pml}} = \begin{bmatrix} 0 & 0 & \rho_0(1+\frac{\sigma_x}{i\omega}) & 0 & 0 \\ 0 & 0 & 0 & 0 & 0 \\ 0 & 0 & 0 & 0 & \frac{(1+\frac{\sigma_x}{i\omega}}{\rho_0} \\ 0 & 0 & 0 & 0 & 0 \\ 0 & 0 & \gamma p_0(1+\frac{\sigma_x}{i\omega}) & 0 & 0 \end{bmatrix},$$

$$[C]_{\text{pml}} = \begin{bmatrix} i\omega+\sigma_D & \overline{\sigma}_x\rho_0(1+\frac{\sigma_r}{i\omega}) & \frac{\rho_0}{r}\frac{\sigma_x}{i\omega} & \rho_0\frac{i\omega}{r}(1+\frac{\sigma_{x,r}}{i\omega}) & 0 \\ 0 & i\omega+\sigma_D & 0 & 0 & \overline{\sigma}_x\rho_0(1+\frac{\sigma_r}{i\omega}) \\ 0 & 0 & i\omega+\sigma_D & 0 & 0 \\ 0 & 0 & 0 & i\omega+\sigma_D & \frac{1}{\rho_0}\frac{im}{r}(1+\frac{\sigma_{x,r}}{i\omega}) \\ 0 & \overline{\sigma}_x\gamma p_0(1+\frac{\sigma_r}{i\omega}) & \frac{\gamma p_0}{r}(1+\frac{\sigma_x}{i\omega}) & \gamma p_0\frac{i\omega}{r}(1+\frac{\sigma_{x,r}}{i\omega}) & i\omega+\sigma_D \end{bmatrix} \quad (2.11)$$

where $\sigma_D = \sigma_{x,r} + \overline{\sigma}_x u_0(1+\frac{\sigma_r}{i\omega})$; $\sigma_{x,r} = \sigma_x + \sigma_r + \frac{\sigma_x\sigma_r}{i\omega}$; $\overline{\sigma}_x = \frac{\sigma_x}{c_0}\frac{M_0}{1-M_0^2}$; and $M_0 = u_0/c_0$. The damping constants σ_x and σ_r are of the same units as ω and are given by

$$\sigma_x = (1-M_0^2)\frac{c_0}{L_{ref}}\sigma_{x,max}\left|\frac{x-x_i}{L_x}\right|^\beta \quad (2.12)$$

$$\sigma_r = \frac{c_0}{L_{ref}}\sigma_{r,max}\left|\frac{r-r_i}{L_r}\right|^\beta \quad (2.13)$$

where c_0 is the speed of sound in the PML, L_{ref} is a reference length, L_x and L_r are the widths of the PML in the x and r-directions, respectively, and x_i and r_i are the locations of the interfaces between the PML and Euler domains in the x and r directions, respectively. The value of β is usually taken as 2, and $\sigma_{max}\Delta x/L_{ref}$ is usually set to 2.

In order to excite the field with sources from the duct inlets, the PML equations are applied to the reflected wave components. Assuming the total acoustic field is composed of an incident field plus the reflected waves, $\hat{\mathbf{q}} = \hat{\mathbf{q}}_{in} + \hat{\mathbf{q}}_{re}$,

$$[A]_{\text{pml}}\frac{\partial\{\hat{\mathbf{q}}\}}{\partial x} + [B]_{\text{pml}}\frac{\partial\{\hat{\mathbf{q}}\}}{\partial r} + [C]_{\text{pml}}\{\hat{\mathbf{q}}\} = [A]_{\text{pml}}\frac{\partial\{\hat{\mathbf{q}}_{\text{in}}\}}{\partial x} + [B]_{\text{pml}}\frac{\partial\{\hat{\mathbf{q}}_{\text{in}}\}}{\partial r} + [C]_{\text{pml}}\{\hat{\mathbf{q}}_{\text{in}}\} \quad (2.14)$$

where subscript 'in' refers to the incident field. This field is constructed using cylindrical duct eigensolutions obtained from the solution of convected wave equation for pressure perturbation.

The velocity perturbations are obtained by substituting the pressure solution into the linearized Euler equations. This procedure gives

$$\begin{aligned}
\hat{p}_{\text{in}} &= \sum_{\mu} A^{+}_{m\mu}\left[J_m(k_{m\mu}r) + Q_{m\mu}Y_m(k_{m\mu}r)\right]\exp[i(-k^{+}_{x,m\mu}x + m\theta)] \\
\hat{\rho}_{\text{in}} &= \tilde{\rho}\exp(-ik_{x,m\mu}) = \hat{p}/c_0^2 \\
\hat{u}_{\text{in}} &= \tilde{u}\exp(-ik_{x,m\mu}) = \frac{k^{+}_{x,m\mu}\hat{p}}{\rho_0(\omega - u_0 k^{+}_{x,m\mu})} \\
\hat{v}_{\text{in}} &= \tilde{v}\exp(-ik_{x,m\mu}) = -\frac{\partial\hat{p}/\partial r}{i\rho_0(\omega - u_0 k^{+}_{x,m\mu})} \\
\hat{w}_{\text{in}} &= \tilde{w}\exp(-ik_{x,m\mu}) = -\frac{\partial\hat{p}/\partial\theta}{i\rho_0 r(\omega - u_0 k^{+}_{x,m\mu})}
\end{aligned} \tag{2.15}$$

where $k^{+}_{x,m\mu}/k = [-M + \sqrt{1-(1-M^2)(k_{m\mu}/k)^2}]/(1-M^2)$ with $k = \omega/c_0$; $A_{m\mu}$ is a constant; J_m and Y_m are the mth order Bessel functions of the first and second kind, respectively; $Q_{m\mu} = Y'_m(\sigma k_{m\mu} r_{\text{tip}})/J'_m(\sigma k_{m\mu} r_{\text{tip}})$, and $\sigma = r_i/r_o$ (ratio of inner and outer radii), and μ is the radial mode order.

2.3.2 Far-field Boundary Conditions

Two different far-field boundary conditions are used during this study. The Perfectly Matching Layer approach developed by Hu is applied to the current problem as described above. As another option Asymptotic Characteristic Based boundary condition by Tam and Webb are also used [13].

2.3.2.1 Asymptotic Characteristic Based Boundary Condition

Due to the convergence problems occurred while using PML approach characteristic based boundary condition applied by Ulusoy [6] is also used as the far-field boundary condition. Non-reflecting boundary conditions are embedded on the outer far-field boundaries. The outgoing waves are damped. The first order spherical damper condition of Bayliss and Turkel [12], *the radiation B*1 *operator*, is used on the inflow parts of these boundaries. On the outflow parts, the linearized momentum equations are solved for the velocity perturbations, but the radiation operator is applied to the pressure perturbation as suggested by Tam and Webb [13]. All farfield

boundary conditions are also transformed to the frequency domain in cylindrical coordinates. The B1 operator is arranged as in Equation 2.16.

$$B_1 = \frac{1}{c_\infty \beta}(1 - \frac{x}{d}\frac{M_\infty}{\beta})\frac{\partial}{\partial t} + \frac{x}{t}\frac{\partial}{\partial x} + \frac{r}{d}\frac{\partial}{\partial r} + \frac{1}{d}$$
$$\beta = \sqrt{1 - M^2}$$
$$d = \sqrt{(x^2/\beta^2) + r^2} \tag{2.16}$$

2.4 Background Flow Modelling

It is crucial to model the shear layer effect on the flow field since the diffraction and refraction behavior of the sound radiating throughout the exhaust nacelles is directly related to the nonuniform velocity gradient in the mixing layer. The code developed within this study has 3 different methods to obtain the background flow field. These are:

- Importing CFD results obtained by commercial codes for more realistic solutions of complex geometries like generic engine geometry.
- Computing background flow field using artificial shear layer model growing from the trailing edge of exhaust nacelles.
- Modelling background flow field using infinitely thin shear layer approach.

2.4.1 Artificial Shear Layer Model

Artificial shear layer definition is based on an error function that transfers the flow quantities from one side of the jet to the other. Analytical shear layer model for free jets is used since the background flow is assumed to be uniform. The model is define by Schlichting [14] as;

$$u = \frac{U_1 + U_2}{2}\left[1 + \frac{U_1 - U_2}{U_1 + U_2} erf\zeta\right] \tag{2.17}$$

where, U_1 and U_2 define uniform flow velocities of the outer and inner jet streams and x, y relatively distance from the trailing edge of duct wall in axial, radial directions. Additionally,

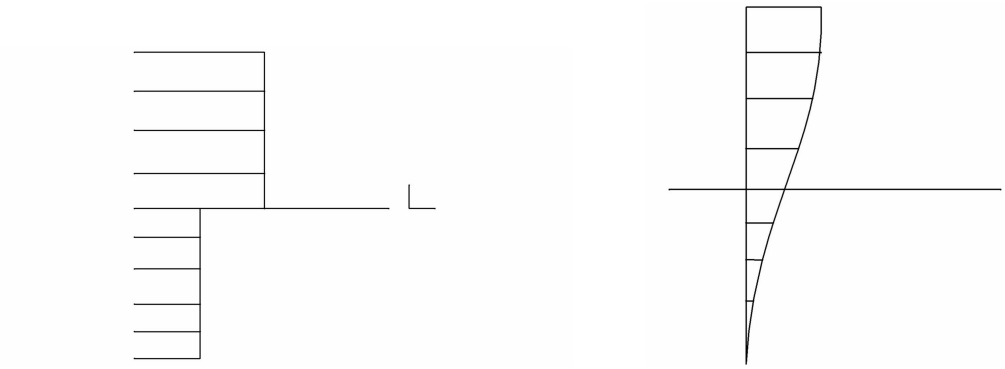

(a) Infinitely Thin Shear Layer With Uniform Flow (b) Artificial Shear Layer

Figure 2.5: Shear Layer Velocity Profiles.

$$\zeta = \sigma \frac{y}{x} \tag{2.18}$$

as Schlichting states $\sigma = 13.5$ when the shear layer expansion cone angle θ as shown in fig. 2.6 is 7^o.

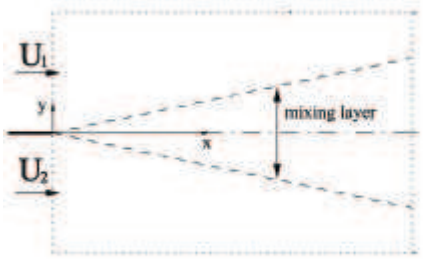

Figure 2.6: Mixing Layer.

2.5 Far-field Predictions

A modified version of the Kirchhoff method is employed for far-field sound calculation. The method, given by Farassat and Myers [15] has been transformed to frequency domain and used by the present code. Kirchhoff method is applied for converged solutions by the construction of a 3-D Kirchhoff surface. This surface is constructed by revolving a set of grid lines 360^o around the engine axis. Then the data on the Kirchhoff surface is integrated for specified far-field observer locations. The frequency domain form of Kirchhoff formula used in the present code

is given by,

$$4\pi\widehat{p_a}(x,w) = \int\int_S \left[\frac{E_1}{R(1-M_R)} + \frac{\widehat{p_a}E_1}{R^2(1-M_R)}\right] e^{-ikR}\, dS \tag{2.19}$$

where $R = |\overrightarrow{R}|$ is the distance between the Kirchhoff surface and observer, $M_R = \overrightarrow{M} \cdot \frac{\overrightarrow{R}}{R}$, and

$$E_1 = -\overrightarrow{n} \cdot \bigtriangledown \widehat{p_a} + (\overrightarrow{M} \cdot \overrightarrow{n})(\overrightarrow{M} \cdot \bigtriangledown \widehat{p_a}) + \left[\frac{\cos\varphi - \overrightarrow{M} \cdot \overrightarrow{n}}{c_\infty(1-M_R) - \frac{\overrightarrow{M} \cdot \overrightarrow{n}}{c_\infty}}\right] i\omega\widehat{p_a}$$

$$E_2 = \left(\frac{1-M}{(1-M_R)^2}\right)(\cos\varphi - \overrightarrow{M} \cdot \overrightarrow{n}) \tag{2.20}$$

$$R = \frac{-(x_1 - y_1)M_\infty + \sqrt{(x_1-y_1)^2 + \beta^2(x_2-y_2)^2}}{\beta^2} \tag{2.21}$$

where, $\beta^2 = 1 - M_\infty^2$, (x_1, x_2) observer location relatively in axial and radial directions and (y_1, y_2) surface location relatively in axial and radial directions.

CHAPTER 3

NUMERICAL METHOD

3.1 Discretization

It is known that the dispersion characteristics of the discretization scheme is critical in CAA applications. Therefor, high order algorithms are preferred. The 4th-order standard finite difference scheme is used for the problems investigated in this thesis. In the interior of solution domain centeral differencing is used, while near or at the boundaries biased differencing is used. The stencil of the centeral scheme is shown in fig. 3.1. The stencils used near or at the boundaries are shown in fig. 3.2

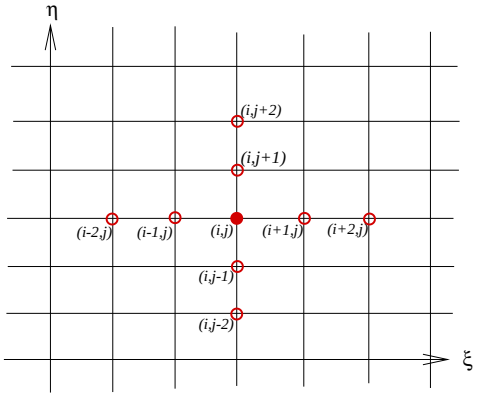

Figure 3.1: Fourth Order Finite Difference Stencil

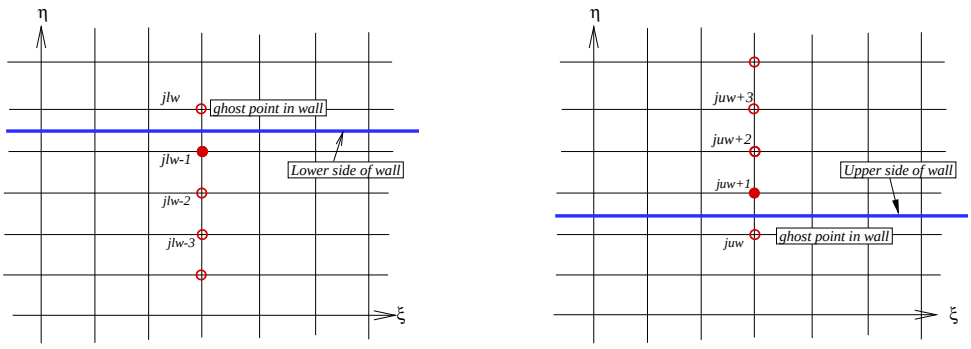

(a) Lower Edge of Hard Wall

(b) Upper Edge of Hard Wall

Figure 3.2: Third Order Finite Difference Stencil.

3.2 Pseudo-Time Derivative Approach

In order to solve the frequency domain equations iteratively, a pseudo time derivative is introduced into the equations. Then, these equations can be solved using a standard time integration technique. With steady boundary conditions the discretized form of these equations are marched in time driving the pseudo time derivative to zero. Hence, a solution to the original equations is obtained.

During this study two different time integration methods are used. First, an alternating direction implicit (ADI) method is applied to solve the discretized equations that are given by the FLESTURN code [9]. This code employs the PML boundary conditions. Second, fully explicit 4-stage Runge-Kutta (RK-4) method is employed in a separate code which uses asymptotic based characteristic boundary conditions. In this study it has been found that the pseudo time integration techniques applied to the model using the PML conditions fail to converge. Therefore, the results obtained using the RK-4 tehcnique will be presented.

3.2.1 ADI Time Integration Method

Alternating Direction Implicit method is applied to the system of equations defining the problem as shown in eqn. 3.1. The aim of using ADI is to decrease band-width while still preserving the implicit character of the equations in at least one of the coordinate directions. This may help suppressing the convective instabilities that are supported by the LEE. When the pseudo

time derivative is added, the equation system becomes,

$$\frac{\partial \mathbf{q}}{\partial \tau} + [A]\frac{\partial \mathbf{q}}{\partial \xi} + [B]\frac{\partial \mathbf{q}}{\partial \eta} + [C]\mathbf{q} = \mathbf{Rhs} \tag{3.1}$$

where $[A]$, $[B]$, $[C]$ represents Jacobian matrices of the governing equations and the farfield boundary conditions in curvilinear co-ordinates, and $\partial \mathbf{q}/\partial \tau$ is the pseudo-time derivative. The ADI method can be written as,

In η-direction :

$$\frac{\partial \mathbf{q}^{n+\frac{1}{2}}}{\partial \tau} + [A]\frac{\partial \mathbf{q}^{n}}{\partial \xi} + [B]\frac{\partial \mathbf{q}^{n+\frac{1}{2}}}{\partial \eta} + [C]\mathbf{q}^{n+\frac{1}{2}} = \mathbf{Rhs} \tag{3.2}$$

where,

$$\frac{\partial \mathbf{q}^{n+\frac{1}{2}}}{\partial \tau} = \frac{\mathbf{q}^{n+\frac{1}{2}} - \mathbf{q}^{n}}{\triangle \tau/2} \tag{3.3}$$

Substituting 3.3 into 3.2, and discretizing the spatial derivatives the resulting linear system of the equations can be written.

$$\left(\frac{1}{\triangle \tau/2}[I] + [OpB] + [C]_{exp} + [C]_{imp}\right)\mathbf{q}^{n+\frac{1}{2}} = \left(\frac{1}{\triangle \tau/2}[I] - [OpA]_{exp} - [OpA]_{imp}\right)\mathbf{q}^{n} + \mathbf{Rhs} \tag{3.4}$$

In ξ-direction :

$$\frac{\partial \mathbf{q}^{n+1}}{\partial \tau} + [A]\frac{\partial \mathbf{q}^{n+1}}{\partial \xi} + [B]\frac{\partial \mathbf{q}^{n+\frac{1}{2}}}{\partial \eta} + [C]\mathbf{q}^{n+1} = \mathbf{Rhs} \tag{3.5}$$

where,

$$\frac{\partial \mathbf{q}^{n+1}}{\partial \tau} = \frac{\mathbf{q}^{n+1} - \mathbf{q}^{n+\frac{1}{2}}}{\triangle \tau/2} \tag{3.6}$$

Substituting 3.6 into 3.5 and splitting the explicit and implicit parts of coefficient matrices $[A]$ and $[C]$. By splitting into explicit and implicit parts the band-width of the sparse matrices $[A]$ and $[C]$ is decreased which improves the convergence speed and the memory requirement for solution of the problem.

$$\left(\frac{1}{\triangle\tau/2}[I] + [OpB] + [OpA]_{imp} + [C]_{imp}\right)\mathbf{q}^{n+1} = \left(\frac{1}{\triangle\tau/2}[I] - [OpA]_{exp} - [C]_{exp}\right)\mathbf{q}^{n+\frac{1}{2}} + \mathbf{Rhs} \tag{3.7}$$

where superscript n shows the iteration step, $\triangle\tau$ is the pseudo-time step size from an iteration step to next, $[OpA]$ is discretized form of $[A]\frac{\partial}{\partial\xi}$ and $[OpB]$ is discretized form of $[B]\frac{\partial}{\partial\eta}$

3.2.2 Fully Explicit Time Integration Method

Numerical experimentation has shown that the PML equations are unstable with ADI method. Therefore, pseudo-time integration method is applied to the problem. Fully explicit, compact, 4-stage Runge-Kutta (RK-4) method is applied to the system of equations defining the problem as shown in eqn. 3.1. Fully explicit method is applied as follows:

$$\frac{\partial\mathbf{q}^{n+1}}{\partial\tau} + [A]\frac{\partial\mathbf{q}^{n}}{\partial\xi} + [B]\frac{\partial\mathbf{q}^{n}}{\partial\eta} + [C]\mathbf{q}^{n} = \mathbf{Rhs} \tag{3.8}$$

Discretizing the spatial derivatives this equation may be written

$$\frac{\partial\mathbf{q}^{n+1}}{\partial\tau} + [A]_{global}\mathbf{q}^{n} = \mathbf{Rhs} \tag{3.9}$$

where $[A]_{global} = [OpA] + [OpB] + [C]$ with $[OpA]$ being the discretized form of $[A]\frac{\partial}{\partial\xi}$, and $[OpB]$ being the discretized form of $[B]\frac{\partial}{\partial\eta}$. RK-4 method is applied as follows:

$$\begin{aligned}
\mathbf{k}_1 &= \mathbf{Rhs} - [A]_{global}\mathbf{q}^{n} \\
\mathbf{q}^{n+\frac{1}{4}} &= \mathbf{q}^{n} + \frac{1}{4}\triangle\tau\mathbf{k}_1 \\
\mathbf{k}_2 &= \mathbf{Rhs} - [A]_{global}\mathbf{q}^{n+\frac{1}{4}} \\
\mathbf{q}^{n+\frac{1}{3}} &= \mathbf{q}^{n} + \frac{1}{3}\triangle\tau\mathbf{k}_2 \\
\mathbf{k}_3 &= \mathbf{Rhs} - [A]_{global}\mathbf{q}^{n+\frac{1}{3}} \\
\mathbf{q}^{n+\frac{1}{2}} &= \mathbf{q}^{n} + \frac{1}{2}\triangle\tau\mathbf{k}_3 \\
\mathbf{k}_4 &= \mathbf{Rhs} - [A]_{global}\mathbf{q}^{n+\frac{1}{2}} \\
\mathbf{q}^{n+1} &= \mathbf{q}^{n} + \triangle\tau\mathbf{k}_4
\end{aligned} \tag{3.10}$$

where superscript n shows the iteration step, $\triangle\tau$ is the pseudo-time step size from an iteration step to the next.

3.3 Parallel Processing Strategy

Solution domain is decomposed into subdomains for parallel processing. The MPI library is used for communication among the subdomains. A code which automatically determines the neighborhood, communication, and boundary condition information for each subdomain for fully structured grids is developed to simplify the decomposition process. New communication subroutines were written to enable arbitrary decomposition of the computational domain. An example decomposition is shown in fig. 3.3.

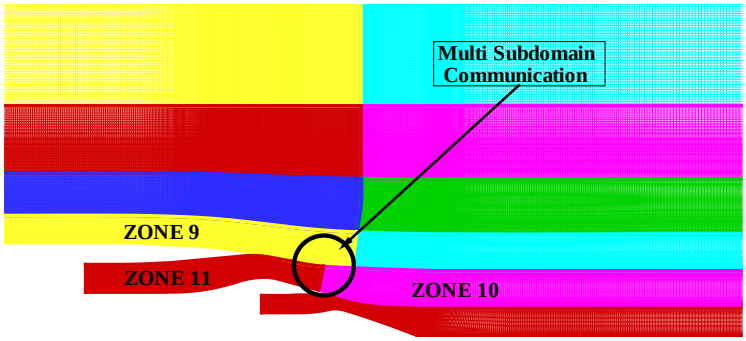

Figure 3.3: Solution Domain of Generic Engine Geometry

CHAPTER 4

RESULTS AND DISCUSSION

4.1 Introduction

For the simulations in this study, two simple duct geometries and a generic engine geometry are considered. These geometries are a circular annular duct geometry, circular co-planar duct geometry, and a generic engine geometry as depicted in fig. 4.1.

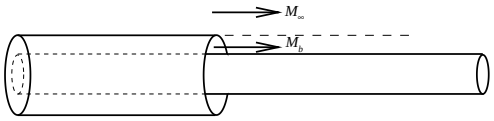

(a) Circular Annular Duct Geometry

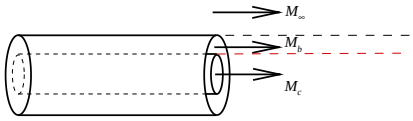

(b) Circular Co-planar Duct Geometry

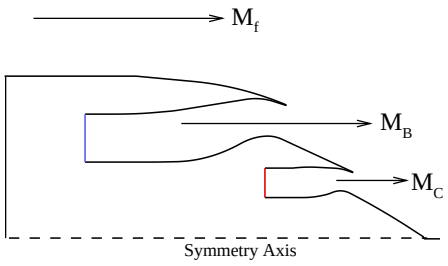

(c) Generic Engine Geometry

Figure 4.1: Test Geometries

In the circular annular duct case, the outer radius of the bypass duct is set to $r_o = 1.2$ m, while the inner radius (which is the radius of the centerbody) is set to $r_i = 0.8$ m. The length of by-pass duct wall L is set such that $L/r_o = 1.667$, while its trailing edge is located at $x = 0$ m. The center body of the circular annular duct case is considered infinitely long.

The outer radius of the bypass duct of the circular co-planar geometry is taken as the outer radius of the previous case. The hub radius of the bypass passage or the outer radius of the inner duct is also the same as the radius of the centerbody of the previous case. However, the duct ends are co-located in the axial direction at $x = 0$.

All the test cases are solved assuming an infinitely thin shear layer first, and then an artificial shear layer that resembles the actual shear layer of the problem. Solutions are also obtained with the artificial shear layer by forcing the mean flow gradients to zero. The mean flow conditions used in these cases are shown in table 4.1, table 4.2 and table 4.3

Table 4.1: Annular Duct Test Cases

	Flight Stream				Bypass Stream			
	M_∞	$T_\infty(K^o)$	$P_\infty(Pa)$	$\rho_\infty(kg/m^3)$	M_B	$T_B(K^o)$	$P_B(Pa)$	$\rho_B(kg/m^3)$
Flight	0.27	288	101325	1.181	0.74	350	101325	0.944

Table 4.2: Co-planar Duct Test Cases

	Flight Stream				Bypass Stream			
	M_∞	$T_\infty(K^o)$	$P_\infty(Pa)$	$\rho_\infty(kg/m^3)$	M_B	$T_B(K^o)$	$P_B(Pa)$	$\rho_B(kg/m^3)$
Flight	0.27	288	101325	1.181	0.74	350	101325	0.944
	Core Stream							
	M_C	$T_C(K^o)$	$P_C(Pa)$	$\rho_C(kg/m^3)$				
Flight	0.5	750	101325	1.084				

Table 4.3: Generic Engine Test Case

	Flight Stream				Bypass Stream			
	M_∞	$T_\infty(K^o)$	$P_\infty(Pa)$	$\rho_\infty(kg/m^3)$	M_B	$T_B(K^o)$	$P_B(Pa)$	$\rho_B(kg/m^3)$
Static	0	288	101325	1.225	0	288	101325	1.225
	Core Stream							
	M_C	$T_C(K^o)$	$P_C(Pa)$	$\rho_C(kg/m^3)$				
Static 0	288	101325	1.225					

In CAA simulations, the mesh quality (mesh resolution, aspect ratio) greatly effects the propagation characteristics such as wave speed and amplitude. Therefore, the mesh must be designed carefully. For the simulations summarized in tables 4.1, 4.2, 4.3 a mesh resolution of

approximately 19 cells per wave length out side the jet (4.2) is used.

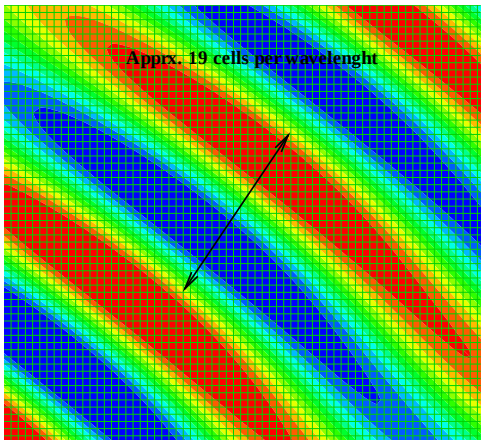

Figure 4.2: Grid Resolution of Co-planar Duct Geometry

Domain decomposition strategy of each test geometry is shown in the following fig. 4.3.

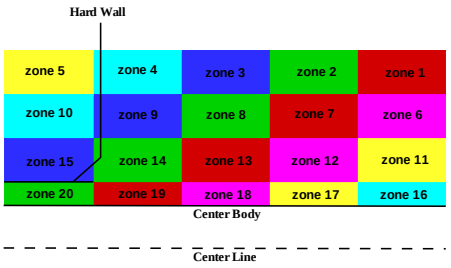

(a) Annular Duct Geometry

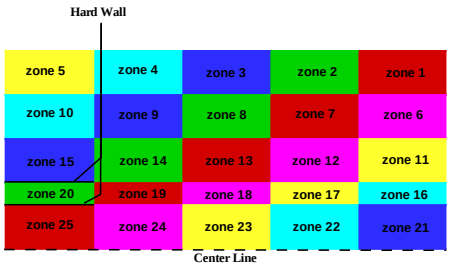

(b) Co-planar Duct Geometry

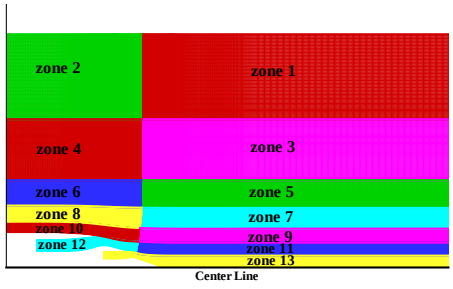

(c) Generic Engine Geometry

Figure 4.3: Domain Decomposition of Test Cases

4.2 Annular Duct, Mode$(0,0)$, $f = 1500Hz$

The computational domain was decomposed into 20 subdomains for the simulation of this case using the three background flow models mentioned in the previous section, The results were obtained in 100000 iterations. The total amount of memory required to solve this problem

turned out to be $20 * 22 = 550$ Mb, which is reasonably small compared to the amount of memory required by the direct solver FLESTURN, which was $2533 * 8 = 20264$ Mb. A total of 9 hours was needed to complete the solution iteratively. This, however, is a much longer time than the cpu time required by FLESTURN, which was 451 seconds.

4.2.1 Results with Infinitely Thin Shear Layer

Contour plots for the mean flow and acoustic fields for the infinitely thin shear layer case are shown in fig. 4.4. It is clear that the jet flow and the exterior flow are uniform and separated from each other with infinitely thin shear layers. The real part of pressure perturbation and sound pressure level (SPL) contour plots shown in fig. 4.4 indicate that convective shear layer instabilities do not appear. This is because the solution approach is based on a cell centered finite difference method and the infinitely thin shear layer lies between two grid points. Hence, all gradients of mean flow, which is uniform for this case, are zero.

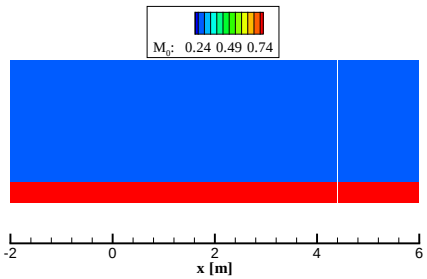

(a) Mean Flow Mach No.

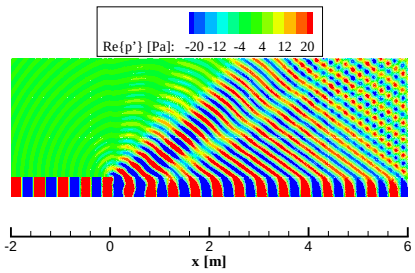

(b) Real Part of Pressure Perturbation

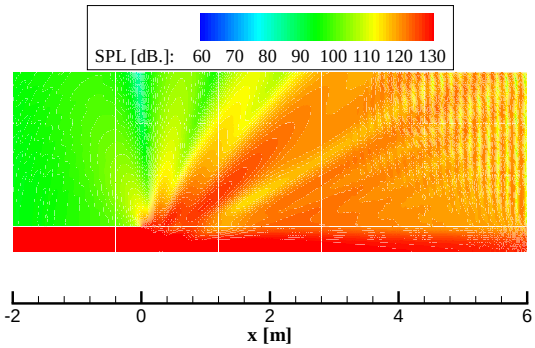

(c) Sound Pressure Level

Figure 4.4: Variable contours of annular duct, Mode$(0, 0)$,$f = 1500Hz$.

Comparison of the SPL distribution obtained by the direct solution approach using FLESTURN and the present iterative method along $r/r_o = 1.25$ constant line (Kirchhoff surface), and

$r/r_o = 1^+$ and $r/r_o = 1^-$ constant lines are shown in fig. 4.5. The latter two constant r lines correspond to the outer and inner sides, respectively, of the by-pass duct and the shear layer emanating from it.

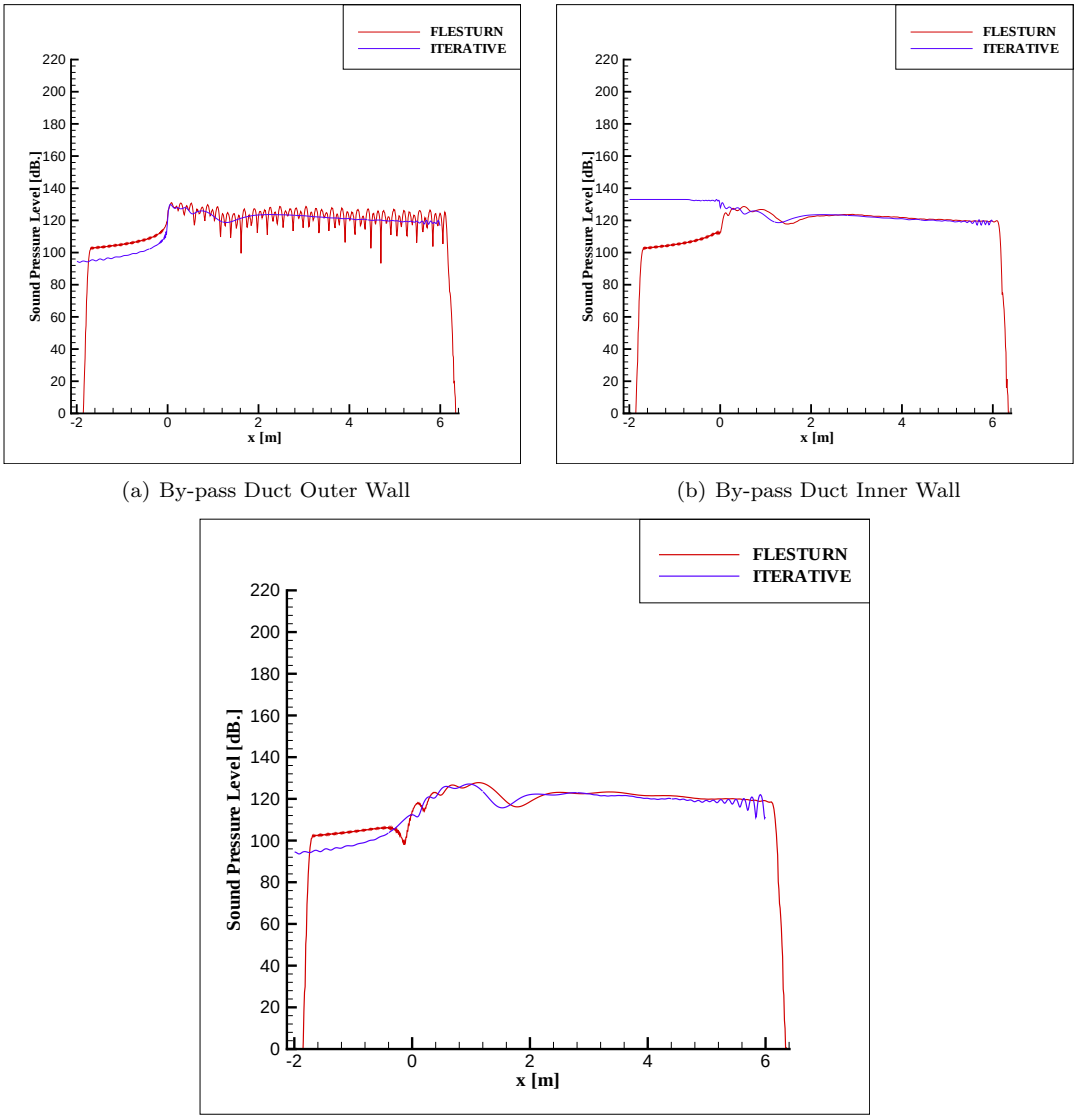

(a) By-pass Duct Outer Wall

(b) By-pass Duct Inner Wall

(c) Kirchhoff Surface

Figure 4.5: Sound pressure level of annular duct, Mode$(0,0)$,$f = 1500Hz$.

As shown in the comparison plots, direct solution and iterative solution methods are compatible with each other for a wide range of axial locations. There occurs a difference in SPL at locations close to the acoustic inlet and far-field boundaries. This difference arises from the fact that the direct solution code and the iterative solution code employ different inlet conditions. The artificial diffusion applied in the iterative solution code is damping the numerical

oscillations, while this is not the case since the direct method does not have artificial diffusion (damping) employed.

4.2.2 Results with Artificial Shear Layer, Mean Flow Gradients Forced to Zero

Contour plots for the mean flow and acoustic fields for this case are shown in fig. 4.6. As seen from the mach contour plot in this figure the jet flow and the exterior flow are mixing into each other generating a growing shear layer. In obtaining the results presented in this section, the mean flow gradients were artificially forced to zero, and therefore, shear layer instabilities were not expected. This is in fact the case, and the real part of pressure perturbation and SPL contour plots indicate that convective shear layer instabilities do not appear.

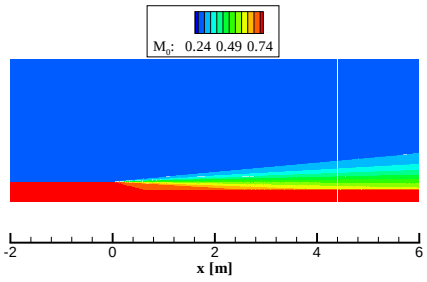

(a) Mean Flow Mach No.

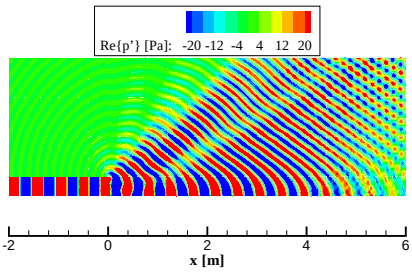

(b) Real Part of Pressure Perturbation

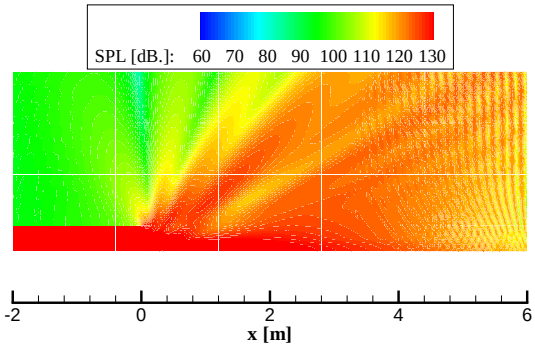

(c) Sound Pressure Level

Figure 4.6: Variable contours of annular duct, Mode$(0,0)$,$f = 1500Hz$.

Comparison of the SPL distribution obtained by the direct solution approach and the present approach along the Kirchhoff surface, and along two lines corresponding to the by-pass duct outer wall and by-pass duct inner wall locations are shown in fig. 4.7. The results plotted agree with each other quite well except near the inlet and farfield boundaries. The reason for this is as has been explained previously.

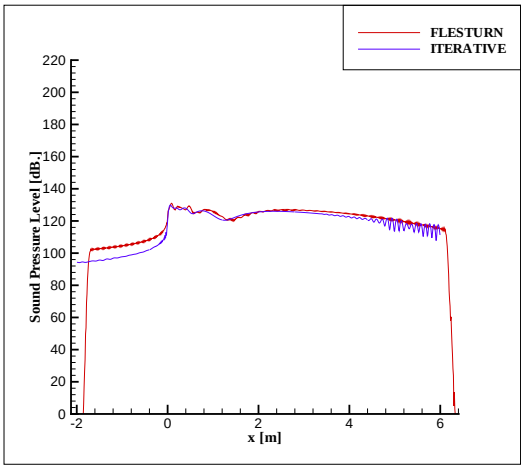

(a) By-pass Duct Outer Wall

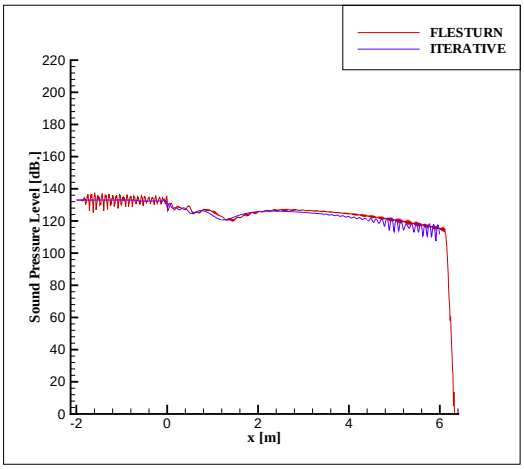

(b) By-pass Duct Inner Wall

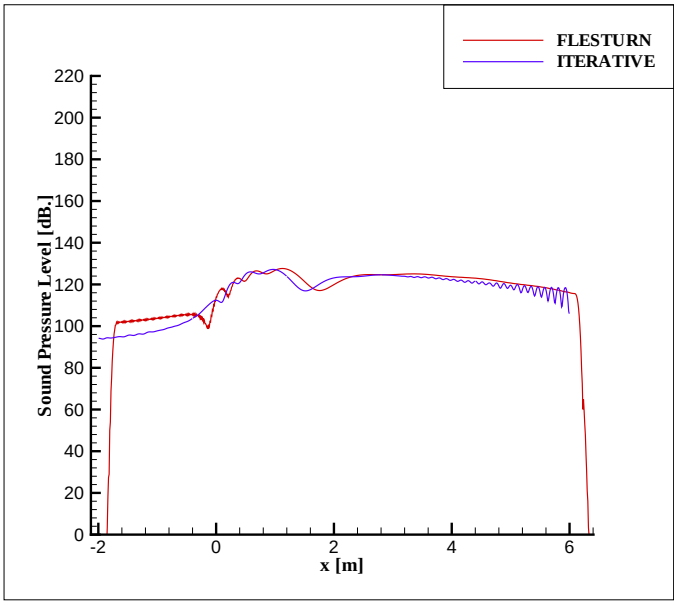

(c) Kirchhoff Surface

Figure 4.7: Sound pressure level of annular duct, Mode$(0,0)$,$f = 1500Hz$.

4.2.3 Results with Artificial Shear Layer, Mean Flow Gradients

Contour plots for the mean flow and acoustic fields for this case are shown in fig. 4.8. Similar to the previous case the shear layer grows in this case. However, the mean flow gradients are retained in the computations. Hence, the convective instabilities may appear in this case. In fact, in the pressure perturbation and SPL contour plots we observe these instabilities.

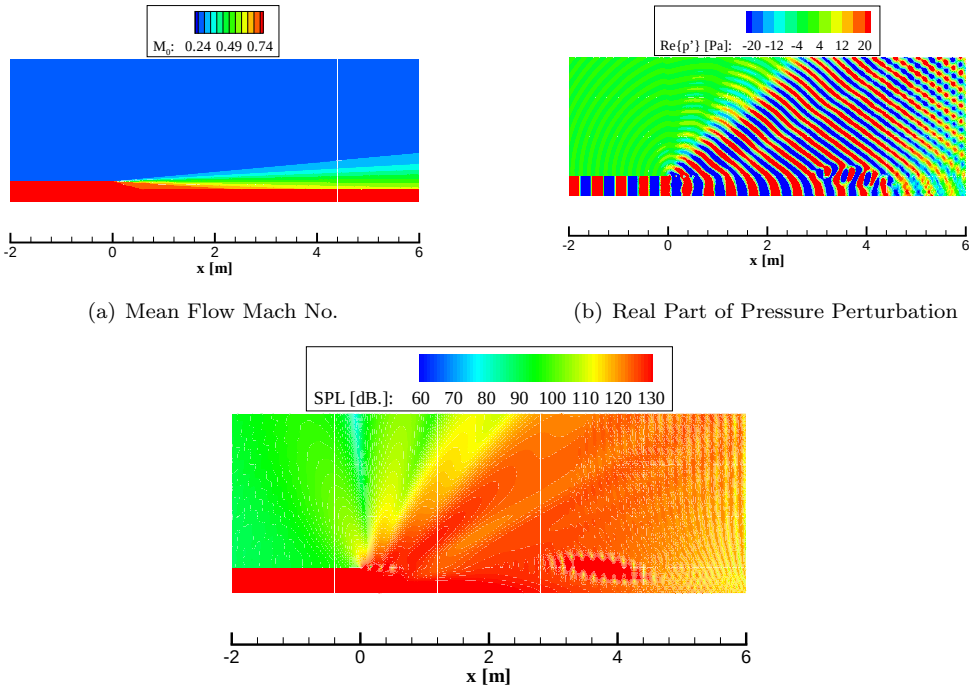

(a) Mean Flow Mach No.

(b) Real Part of Pressure Perturbation

(c) Sound Pressure Level

Figure 4.8: Variable contours of annular Duct, Mode$(0,0), f = 1500Hz$.

The present and FLESTURN solutions are compared along the same r =constant lines in fig. 4.9. There is some disagreement between the two solutions. In addition to the difference due to the artificial damping applied by the present iterative approach, the large SPL difference occurring in the downstream of mixing layer arise due to the shear layer instabilities occur in that region.

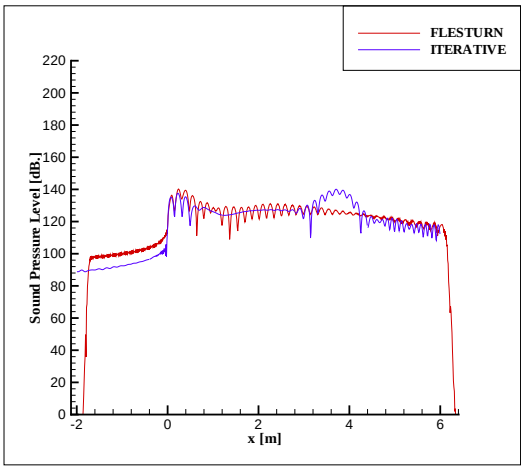

(a) By-pass Duct Outer Wall

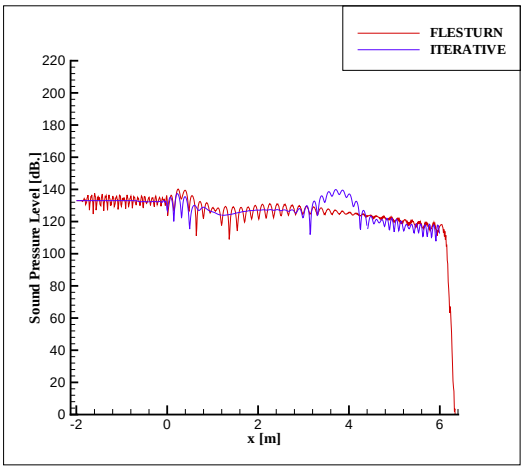

(b) By-pass Duct Inner Wall

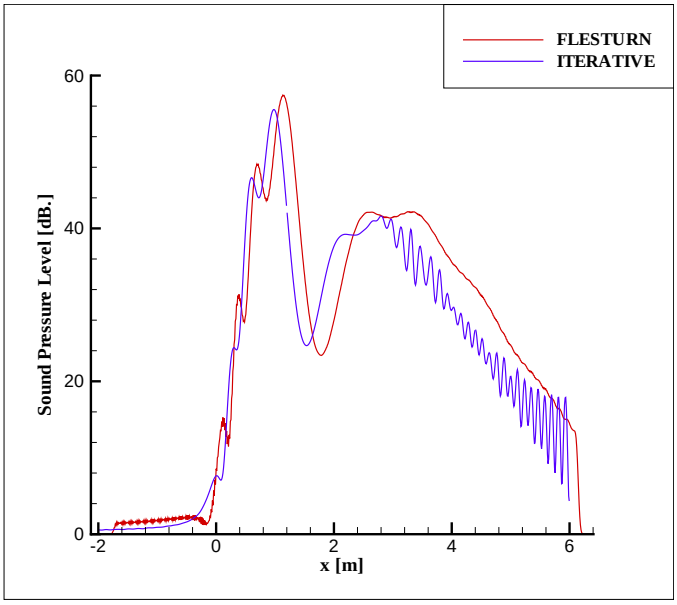

(c) Kirchhoff Surface

Figure 4.9: Sound pressure level of annular duct, Mode$(0,0)$,$f = 1500Hz$.

4.2.4 Influence of Background Flow Fields

A comparison of the SPL distributions obtained using the three mean flow treatments (uniform flow with infinitely thin shear layer, artificially grown shear layer with the gradient terms set to zero, and the artificially grown shear layer with non-zero gradients) is also presented here in fig. 4.10. The distributions show some discrepancies along the walls and in the shear layer, while away from them the agreement between all results is quite good. The reason for the difference has been discussed in the previous individual subsections.

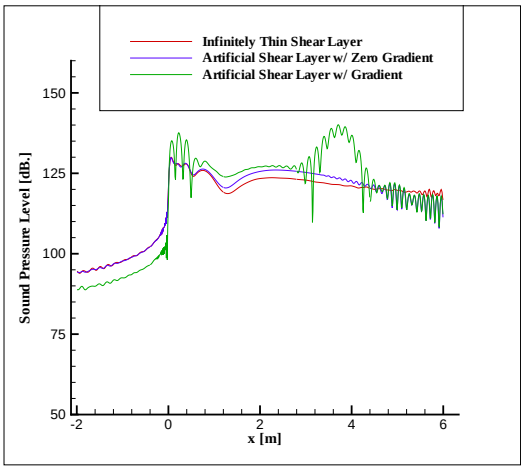

(a) By-pass Duct Outer Wall

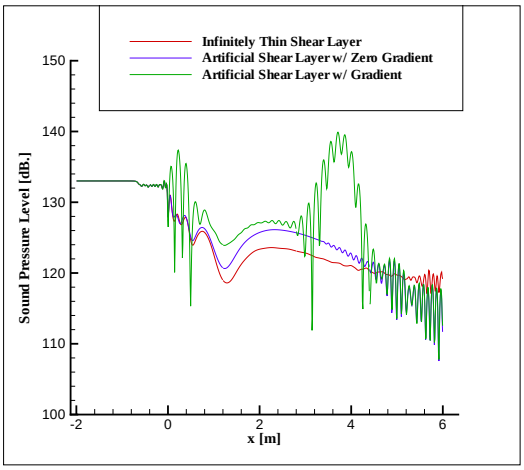

(b) By-pass Duct Inner Wall

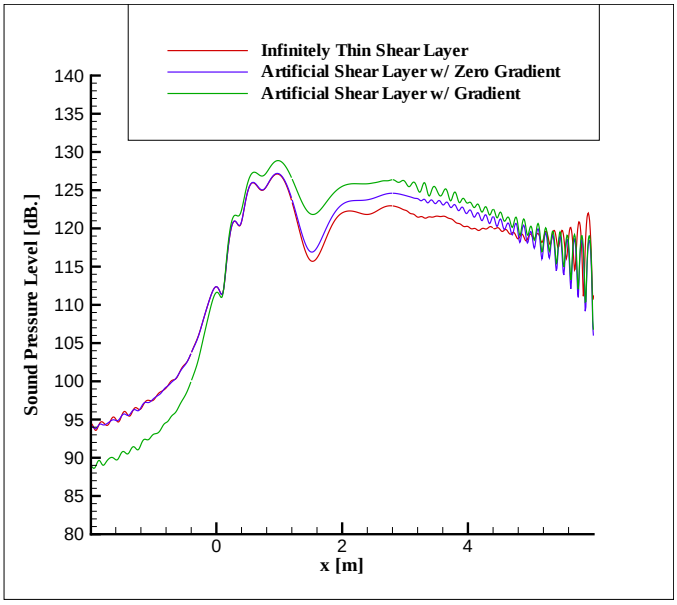

(c) Kirchhoff Surface

Figure 4.10: Sound pressure level of annular duct, Mode$(0,0)$,$f = 1500Hz$.

4.3 Annular Duct, Mode$(21,0)$, $f = 1500Hz$

In this section results for the $(21,0)$ mode at the same frequency as the (0,0) mode are presented. For this case the same computational domain as in the mode$(0,0)$ case is used. The results were obtained in 100000 iterations. Hence, the memory requirement and solution time are also the same as for the previous case discussed above.

4.3.1 Results with Infinitely Thin Shear Layer

The contour plots for the mean flow and acoustic fields for this case are shown in fig. 4.11. As seen from the mach contour plot in this figure, the jet flow and the exterior flow are discontinuous. The contour plots for the real part of pressure perturbation and SPL do not indicate convective shear layer instabilities.

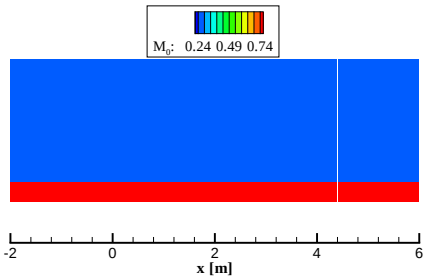

(a) Mean Flow Mach No.

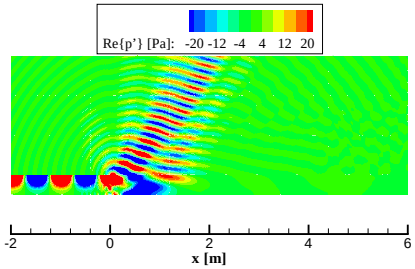

(b) Real Part of Pressure Perturbation

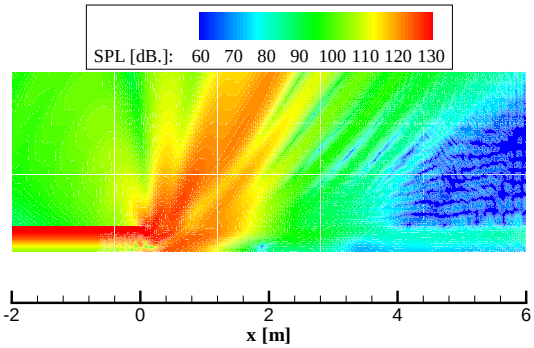

(c) Sound Pressure Level

Figure 4.11: Variable contours of annular duct, Mode$(21, 0)$,$f = 1500Hz$.

4.3.2 Results with Artificial Shear Layer, Mean Flow Gradients Forced to Zero

As opposed to the previous subsection, an artificial shear layer with zero mean gradients is used here. The contour plots for the mean flow and the computed acoustic fields are shown in fig. 4.12. Since the mean flow gradients are artificially forced to zero, shear layer instabilities do not appear in the acoustic pressure contours for the (21,0) mode either.

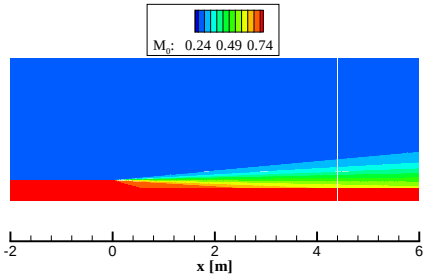

(a) Mean Flow Mach No.

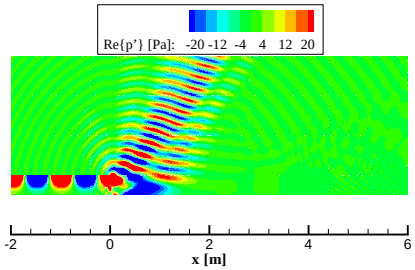

(b) Real Part of Pressure Perturbation

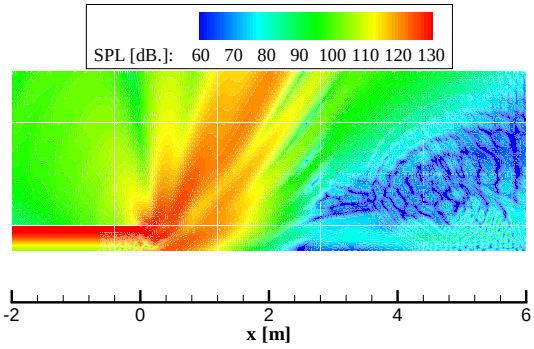

(c) Sound Pressure Level

Figure 4.12: Variable contours of annular duct, Mode$(21, 0)$,$f = 1500Hz$.

4.3.3 Results with Artificial Shear Layer, Mean Flow Gradients

Contour plots for the mean flow and acoustic fields for this case are shown in fig. 4.13. As seen in fig. 4.13 mach contour plot, the jet flow and the exterior flow are mixing into each other continuously. For the computations, the mean flow gradients were kept in the equations. As evident from the real part of pressure perturbation and SPL contour plots shear layer instabilities occur here.

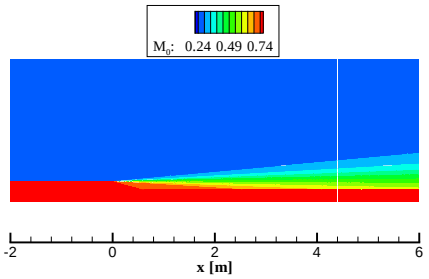

(a) Mean Flow Mach No.

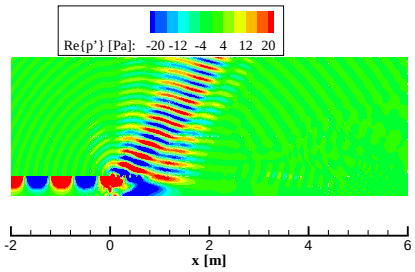

(b) Real Part of Pressure Perturbation

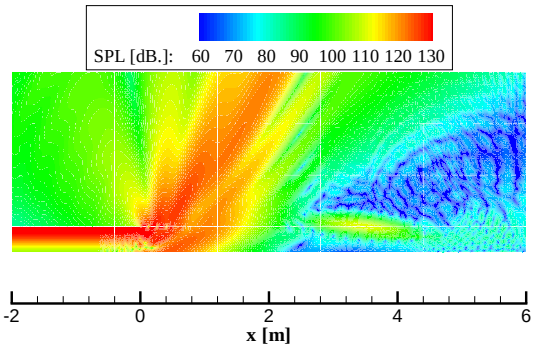

(c) Sound Pressure Level

Figure 4.13: Variable contours of annular Duct, Mode$(21, 0)$,$f = 1500Hz$.

4.3.4 Influence of Background Flow Fields

A comparison of the SPL distribution obtained along the same constant r lines as the previous cases using the three background flow approach solution methods is made in fig. 4.14. Some large differences are observed mainly due to the convective instabilities.

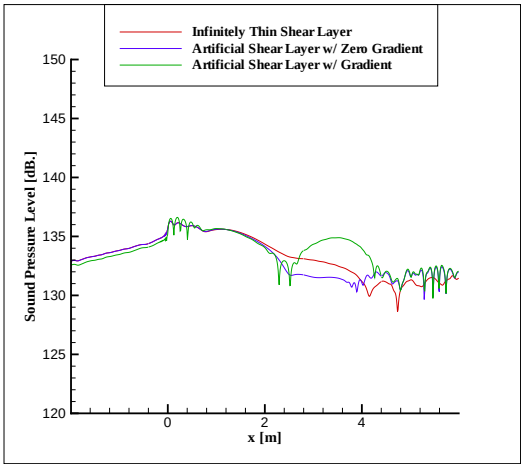

(a) By-pass Duct Outer Wall

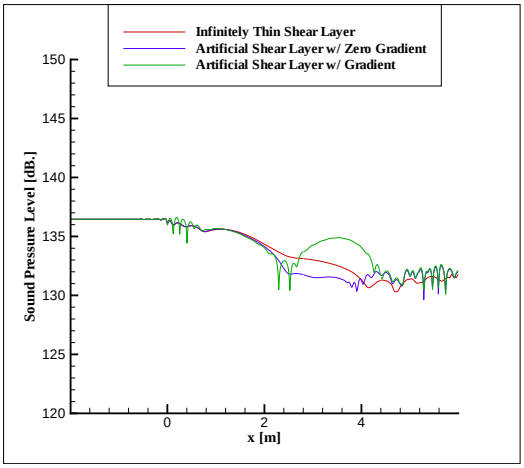

(b) By-pass Duct Inner Wall

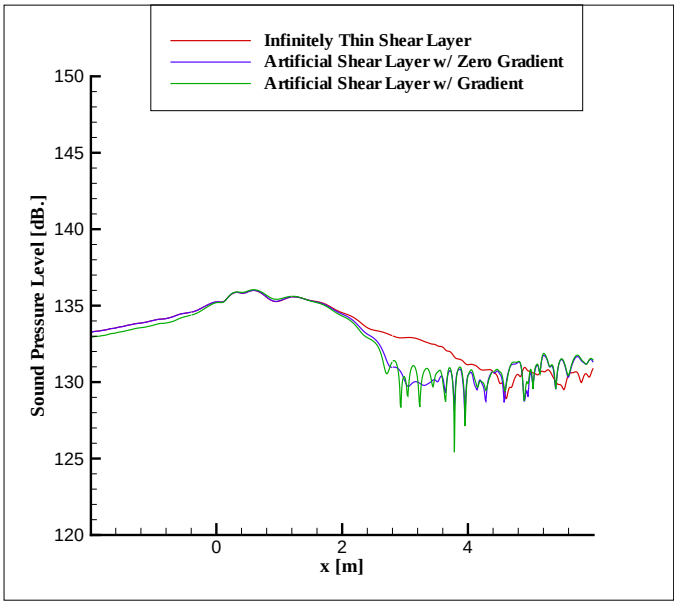

(c) Kirchhoff Surface

Figure 4.14: Sound pressure level of annular duct, Mode$(21, 0), f = 1500Hz$.

4.4 Co-planar Duct, Mode$(0,0)$, $f = 1500Hz$

The computational domain for this case was decomposed into 25 subdomains. The results shown in this section were obtained in 100000 iterations. The total amount of memory required to solve this problem was $25 * 52 = 1300$ Mb. A total of 14 hours was needed to complete the solution iteratively. Acoustic waves were introduced to the solution domain through the by-pass duct. The same modes and frequencies as the previos section were considered. The results indicate similar trends also continue for the co-planar duct case to the annular duct case. The results are given below for the three mean flow treatments.

4.4.1 Results with Infinitely Thin Shear Layer

The contour plots for the mean flow and acoustic fields in fig. 4.15 show that trends of corresponding subsection of annular duct case is similar to this case.

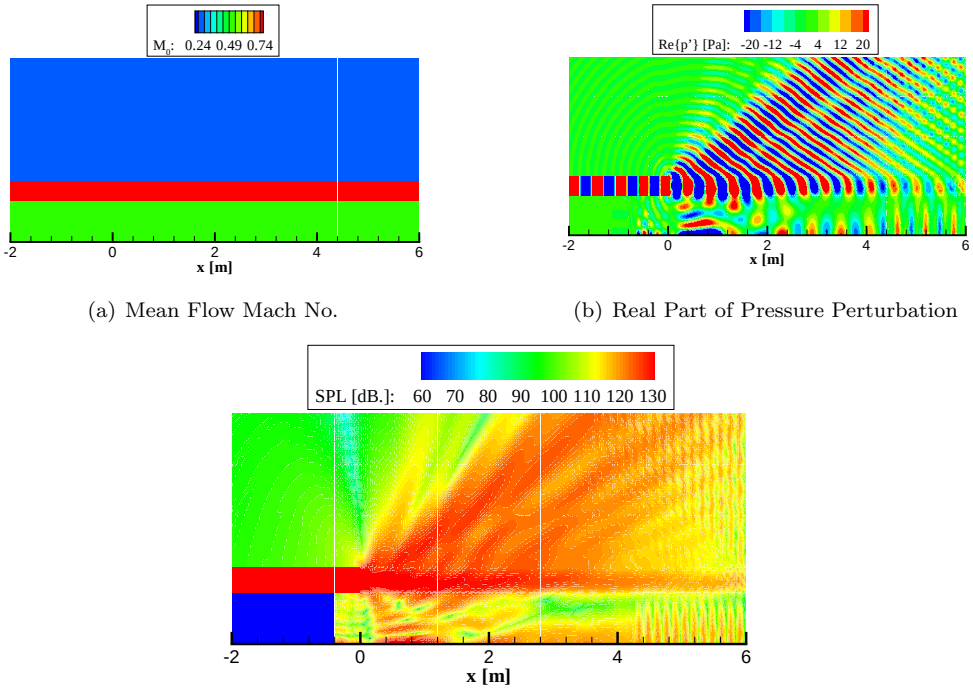

(a) Mean Flow Mach No.

(b) Real Part of Pressure Perturbation

(c) Sound Pressure Level

Figure 4.15: Variable contours of coplanar duct, Mode$(0,0)$,$f = 1500Hz$.

4.4.2 Results with Artificial Shear Layer, Mean Flow Gradients Forced to Zero

Contour plots for the mean flow and acoustic fields for this case are shown in fig. 4.16. It is clear that, similar characteristics are observed in the results of the present case to those of the previous case.

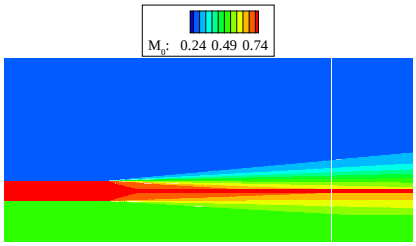

(a) Mean Flow Mach No.

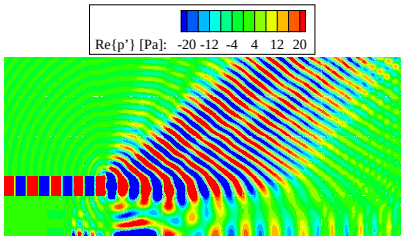

(b) Real Part of Pressure Perturbation

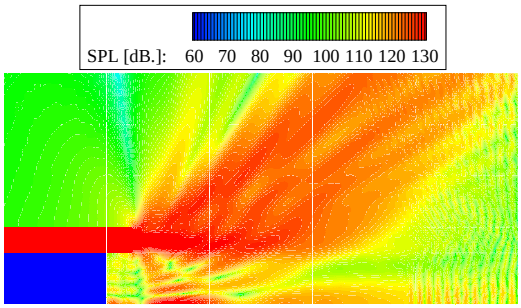

(c) Sound Pressure Level

Figure 4.16: Variable contours of coplanar duct, Mode$(0,0)$,$f = 1500Hz$.

4.4.3 Results with Artificial Shear Layer, Mean Flow Gradients

The contour plots for the mean flow and acoustic fields for this case are shown in fig. 4.17. The results shown follow the same trends as the results obtained for the annular duct case using the artificial shear layer description with non-zero mean flow gradients.

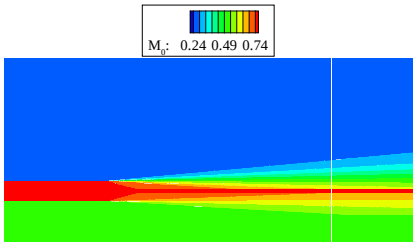

(a) Mean Flow Mach No.

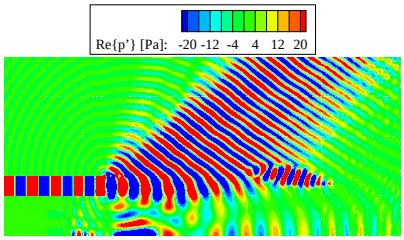

(b) Real Part of Pressure Perturbation

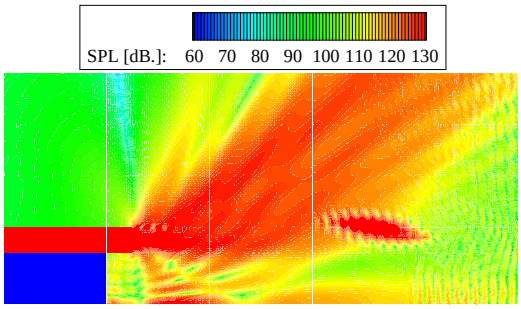

(c) Sound Pressure Level

Figure 4.17: Variable contours of coplanar Duct, Mode$(0,0)$,$f = 1500Hz$.

4.4.4 Influence of Background Flow Fields

The comparison of SPL distribution at three different r =constant lines, which are defined in the beginning of this chapter using the three different background flow approaches employed are shown in fig. 4.18. The results are similar to those obtained for the annular duct case.

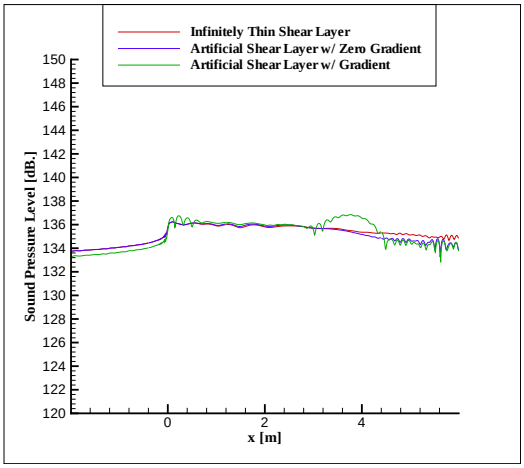

(a) By-pass Duct Outer Wall

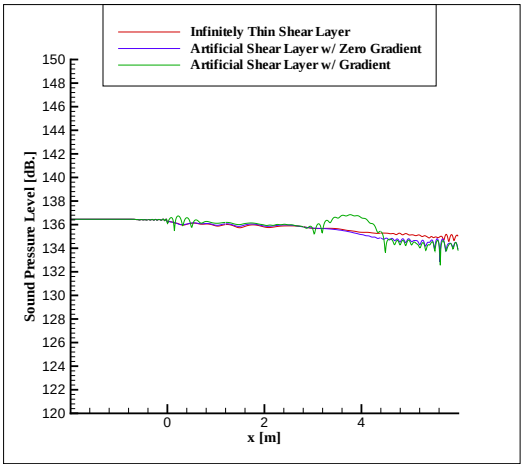

(b) By-pass Duct Inner Wall

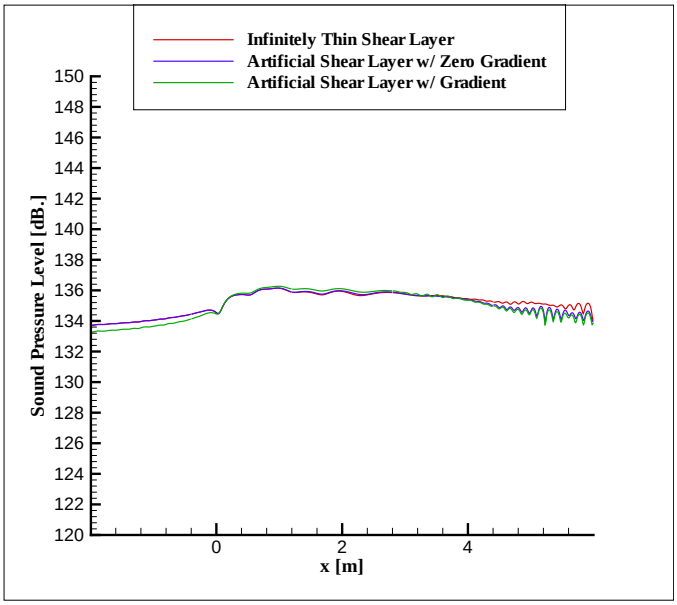

(c) Kirchhoff Surface

Figure 4.18: Sound pressure level of coplanar duct, Mode$(0,0)$,$f = 1500Hz$.

4.5 Co-planar Duct, Mode$(21,0)$, $f = 1500Hz$

In this section results for the $(21,0)$ mode at the same frequency as the (0,0) mode are presented. For this case the same computational domain as in the mode$(0,0)$ case is used. The results were obtained in 100000 iterations. Hence, the memory requirement and solution time are also the same as those for the previous case discussed above. The following results show similar trends for the $(21,0)$ mode case to the $(0,0)$ mode case. The results are given below for the three mean flow treatments.

Figures 4.19, 4.20 and 4.21 show the contour plots for the mean flow and acoustic fields obtained using an infinitely thin shear layer, artificial shear layer with zero mean gradients, and artificial shear layer with non-zero gradients, respectively.

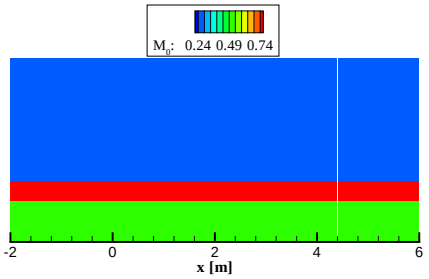

(a) Mean Flow Mach No.

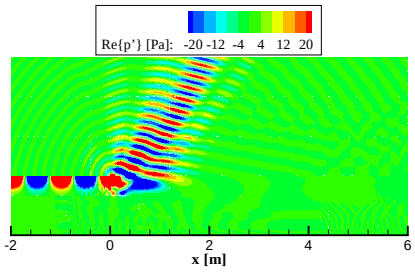

(b) Real Part of Pressure Perturbation

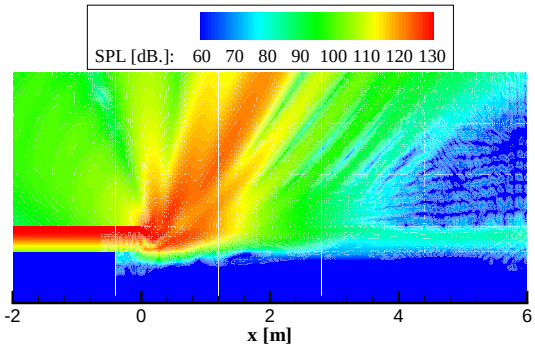

(c) Sound Pressure Level

Figure 4.19: Variable contours of coplanar duct, Mode$(21,0)$,$f = 1500Hz$, Infinitely Thin Shear Layer

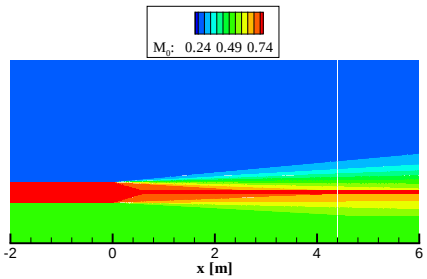

(a) Mean Flow Mach No.

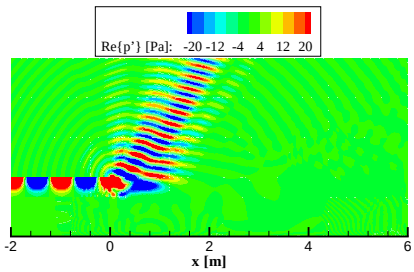

(b) Real Part of Pressure Perturbation

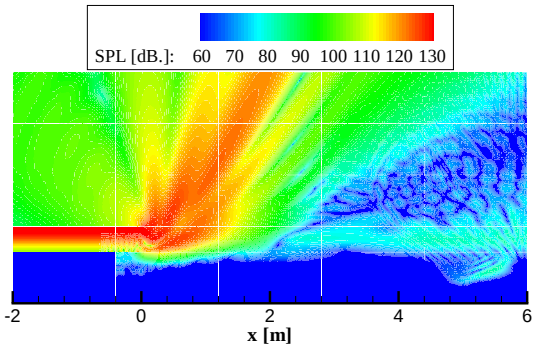

(c) Sound Pressure Level

Figure 4.20: Variable contours of coplanar duct, Mode$(21, 0)$,$f = 1500Hz$, Artificial Shear Layer with Zero Mean Flow Gradients

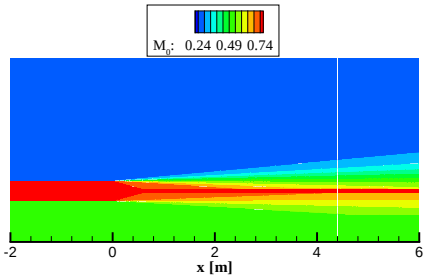

(a) Mean Flow Mach No.

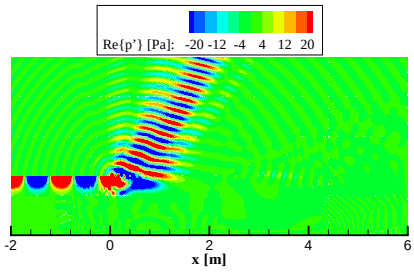

(b) Real Part of Pressure Perturbation

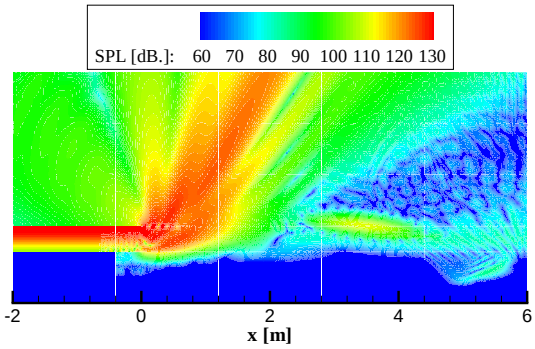

(c) Sound Pressure Level

Figure 4.21: Variable contours of coplanar Duct, Mode$(21, 0)$,$f = 1500Hz$, Artificial Shear Layer with Mean Flow Gradients

The comparison of the SPL distribution at three different r =constant lines, which are same lines used in the previous section using the three different background flow approaches employed are shown in fig. 4.22. The results also follow the same trends as the $(0, 0)$ mode case.

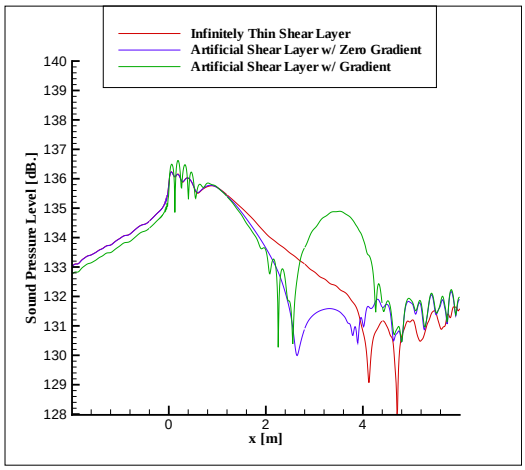

(a) By-pass Duct Outer Wall

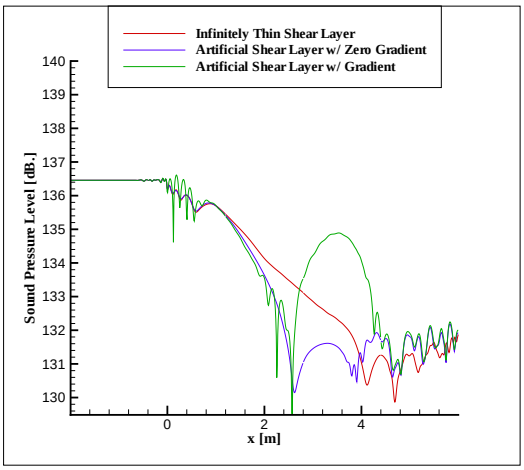

(b) By-pass Duct Inner Wall

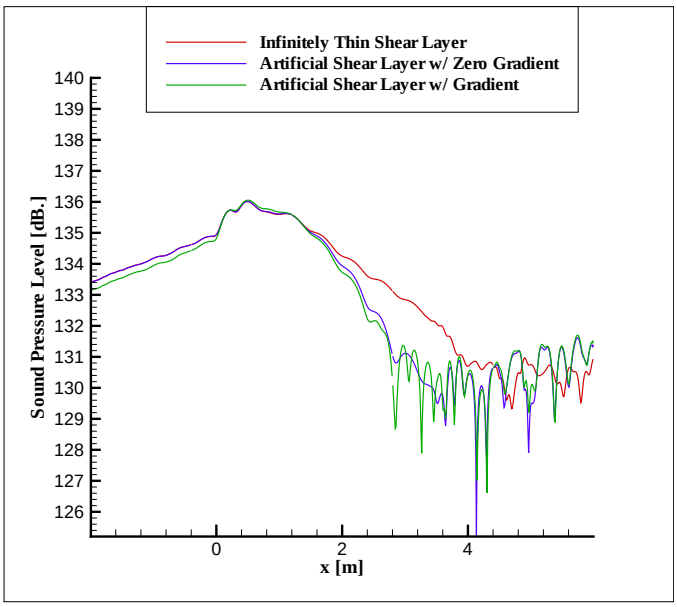

(c) Kirchhoff Surface

Figure 4.22: Sound pressure level of coplanar duct, Mode$(21, 0)$,$f = 1500Hz$.

4.6 Generic Engine, Mode$(11,0)$, $f = 1500Hz$, No Background Flow

In this section, results are obtained for a more realistic geometry for demonstrating the capability of the code to handle non-uniform grids. The computational domain shown in fig. 4.3 for this case was decomposed into 13 subdomains. The results shown below were obtained in 100000 iterations. The total amount of $13 * 54 = 702$ Mb memory, and a total of 28 hours were need to solve this problem. Acoustic waves were introduced to the solution domain only through the by-pass duct. The (11,0) mode is considered at $f = 1500Hz$ without background flow. The resulting acoustic pressure contours are shown in fig. 4.23.

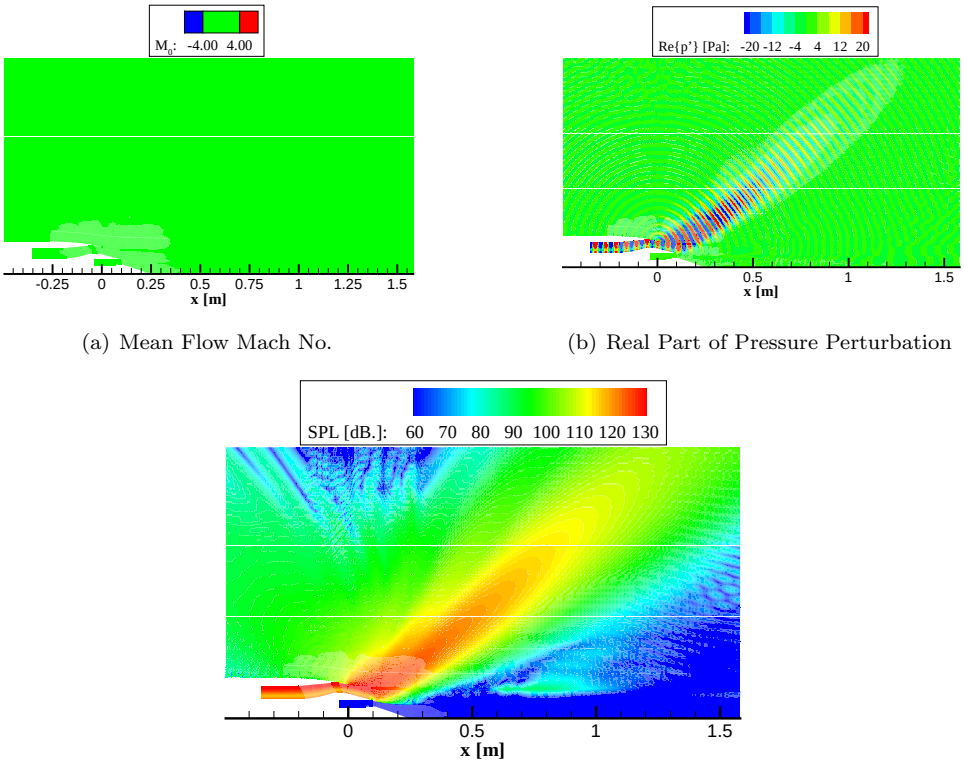

(a) Mean Flow Mach No.

(b) Real Part of Pressure Perturbation

(c) Sound Pressure Level

Figure 4.23: Variable contours of generic engine, Mode$(11,0)$,$f = 1500Hz$.

CHAPTER 5

CONCLUSION

In this thesis, acoustic radiation and propagation problem through a bypass jet is numerically solved in frequency domain employing the linearized Euler Equations as the governing equations. When solved directly the frequency domain formulation eliminates convective instabilities that arise in jet mixing layers mainly due to the radial flow gradients. However, direct solution methods are computationally expensive in terms of computer memory. As a result, a pseudo time derivative term is added to the frequency domain equations so that a time marching technique can be employed, and the solution can be drived to a steady form iteratively. Alternating direction implicit and fully explicit time integration methods are considered as the time marching techniques. The farfield directivity pattern for the propagated sound is calculated using a Kirchhoff formulation. Asymptotic characteristic based boundary conditions and PML techniques are applied to the farfield and wave inlet boundaries. All computations are performed in parallel using the `MPI` library routines.

Numerical results are obtained for three different geometries. These are an annular duct, co-planar duct, and a generic engine geometry. The results for the annular duct geometry are compared with those obtained using the direct solver `FLESTURN`.

In this study three different background flow models are investigated to see assess the numerical behavior of the iterative approach, particularly in terms of the convective instabilities. The mean flow models include an infinitely thin shear layer, an artificial shear layer with mean

flow gradients forced to zero, and an artificial shear layer with mean flow gradients retained. As suggested by Agarwal *et al.* [3] iterative solution to the LEE may also show the Kelvin-Helmholtz type instabilities, and this has been shown in the present study.

It has been shown in this study that, when the mean flow gradients are neglected, the employed iterative approach does not produce convective instabilities, as expected. As stated in chapter 1 the aim of this study was to obtain a more efficient method in terms of computational power to obtain the solution of acoustic propagation and radiation through out the exhaust section without the Kelvin-Helmhotz instability waves. The investigated cases showed that the computer memory requirement of iterative approach was much less then the direct method. Therefore, by suppressing the mean flow gradients, the present iterative approach may be used in parametric study of very high frequency problems, without much computer memory.

REFERENCES

[1] Atlantic Flight Training, *Jeppesen JAR ATPL (A) 2005 Manuals Powerplant Book*, April 2005 press.

[2] Fang, Q. Hu, *Absorbing Boundary Conditions*, International Journal of Computational Fluid Dynamics August 2004 Vol. 18 (6), pp. 513-522.

[3] Agarwal, A., Morris, P.J., Mani, R., *The Calculation of Sound Propagation in Nonuniform Flows: Suppression of Instability Waves*, 41st AIAA Aerospace Sciences Meeting and Exhibit,2003, AIAA 2003-0878

[4] Özyörük, Y., Dizemen, I. E., *Performance Evaluation of Two Parallel, Direct Sparse Solvers for an Aeroacoustic Propagation Model*, Parallel CFD Conference, 2007

[5] Michalke A., *On Spatially Growing Disturbances in an Inviscid Shear Layer* , Journal of Fluid Mechanics, Vol. 23(3), 1965, pp.521-544.

[6] Ulusoy Y.B., *Frequency Domain Computation of Turbofan Exhaust Noise Radiation*, Msc. Thesis METU,(2006)

[7] Özyörük, Y., Dizemen, I. E.,Kaya, S., Aktürk, A., *A Frequency Domain Linearized Euler Solver for Turbomachinery Noise Propagation and Radiation*, 13th AIAA/CEAS Aeroacoustic Conference, 2007, AIAA-2007-3521.

[8] Taylor,J.M. and Sofrin, T.G., *Axial Flow Compressor Studies*, SAE Transactions, Vol.70, 1962, pp. 309-332.

[9] Giles, M.B, *Nonreflecting boundary conditions for Euler Equation Calculation*, AIAA Journal, Vol.28, No.12, 1990, pp.2050-2058.

[10] Özyörük, Y., Alpman, E., Ahuja, V., Long, L.N., *Frequency-Domain prediction of turbofan noise radiation*, Journal of Sound and Vibration, Volume 270, Issue 4-5, pp. 933-950.

[11] Fang, Q. Hu, *Absorbing Boundary Conditions*, International Journal of Computational Fluid Dynamics August 2004 Vol. 18 (6), pp. 513-522.

[12] Bayliss, A., *Far Field Boundary Conditions for Compressible Flows*, Journal of Computational Physics, Vol. 48 (1982), pp. 182-189.

[13] Tam, C.K.W., and Webb, *Dispersion-Relation-Preserving Difference Schemes for Computationla Acoustics*, Journal of Computational Physics, Vol.107, No.2, 1993, pp. 262-281.

[14] Schlichting H., *Boundary Layer Theory*, McGraw-Hill 1979, pp. 738.

[15] Farassat F., Myers M.K., *Extension of Kirchhoff's formula for radiation for moving surfaces*, Journal of Sound and Vibration, Vol. 123, 1988, pp. 451-460.